Analysis of thermodynamics, kinetics, and reaction pathways in the amination of secondary alcohols over Ru/SiO₂

Xin Gao, Dia Sahsah, Andreas Heyden, and Jesse Q. Bond^{1,*}

- ¹ Department of Biomedical and Chemical Engineering, Syracuse University, Syracuse, NY 13244, USA
- ² Department of Chemical Engineering, University of South Carolina, Columbia, SC 29208, USA
- * Address correspondence to: jqbond@syr.edu

Abstract

This work considers the Ru-mediated amination of secondary alcohols with ammonia in vapor and liquid media. We map thermodynamic constraints, and we probe the impacts of species partial pressure, residence time, and reaction temperature on rate, selectivity, and catalyst stability. Alcohol amination consumes no H₂, and H₂ has no significant impact on amination kinetics; however, operating under H₂ benefits Ru stability. Primary amine selectivity increases with ammonia pressure and alcohol conversion, and the latter observation is consistent with the formation of primary amines through a network of sequential reactions. Unfortunately, primary amines are susceptible to secondary deamination to form hydrocarbons. As is typical of processes that seek to isolate a reactive intermediate, the main selectivity challenge here is identifying residence times that are long enough to accumulate high substrate conversion but short enough to avoid secondary deamination. In general, moderate residence times will maximize the production of primary amines. Insights extend across a broad substrate scope, and we observe 70 - 90% yield of primary amines from linear, cyclic, and heterocyclic alcohols. That said, heterocyclic alcohols appear susceptible to product inhibition, so achieving high conversions requires longer residence times and/or increased ammonia pressures.

Keywords

Alcohol amination, Ru, amination kinetics, heterogeneous, primary amines, ammonia

Introduction

Aminations (also called amine alkylations) are reactions that couple ammonia or alkylamines with alkenes, ^{1–5} alcohols, ^{6–10} or carbonyl compounds. ^{11–15} Aminations therefore facilitate the synthesis of primary, secondary, and tertiary amines, which are bases that have applications as catalysts; 16,17 in acid gas cleanup (e.g., CO₂ scrubbing); ¹⁸ and as intermediates in the production of dyes, ^{19–21} pharmaceuticals, ^{22–26} and agrochemicals. ^{27–30} In the context above, "amination" refers to a reaction that forms a bond between an *electrophilic* carbon and a *nucleophilic* nitrogen; thus, the ease of amination is dictated by the relative nucleophilicity of the nitrogen atom and the electrophilicity of the carbon atom.^{31,32} For example, the alkylation of a strong nucleophile, such as the nitrogen atom in a secondary alkylamine, with a strong electrophile, such as the α -carbon in an alkyl halide, can proceed under mild conditions without catalyst addition.³³ In contrast, the addition of a weak nucleophile, such as the nitrogen atom in ammonia, to a weak electrophile, such as the α -carbon in an alcohol, requires activation of either or both substrates. 10 Despite their lack of innate reactivity, ammonia and alcohols are attractive amination feedstocks. Both are relatively inexpensive, and alcohols can often be sourced from biomass.^{34–36} Moreover, alcohol amination is green and atom-efficient: it produces only water as a coproduct, and it consumes no hydrogen.^{37,38} Alcohol amination is therefore intriguing relative to the more common reductive amination of aldehydes or ketones, which consumes one equivalent of dihydrogen per C-N bond formed. 15,39 There are two main catalytic strategies for alcohol amination. Both are geared toward alcohol activation; specifically, they facilitate the amination of a secondary alcohol by increasing the electrophilicity of its α -carbon. We further note that each cataltyic approach is amenable to using ammonia or higher amines as the nitrogen source, but we restrict consideration to ammonia in this

study.^{10,33,40,41} First, acids—either protons or metal cations—will catalyze alcohol amination at high temperatures (300 – 500°C).^{42–44} The major challenge with this approach is that acid sites also catalyze alcohol dehydration and amine deamination, which are difficult to control at elevated temperatures. As such, one observes significant alkene formation during the acid-catalyzed amination of alcohols.^{44–49} Alternatively, metal catalysts can be used to facilitate alcohol amination at 100 – 350°C (Figure 1).^{42,43} The prevailing view is that alcohol amination (Reaction 1) proceeds

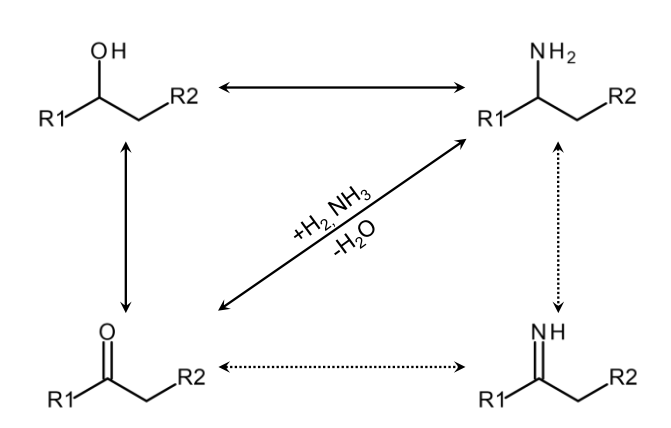


Figure 1: Macroscopic reactions occurring during the amination of secondary alcohols to form primary amines. Pathway (1) represents the formation of a primary amine through direct amination of the alcohol. Pathways (2) and (3) comprise the formation of a primary amine by secondary amination of a ketone formed by dehydrogenation of the alcohol. Solid lines lead to products that are observable under conditions reported here. Dashed lines describe the formation and consumption of imines, which are presumed intermediates in ketone amination.

over metal sites through the so called "borrowing hydrogen" mechanism. 50,51 This involves primary dehydrogenation of the alcohol to form a carbonyl compound and dihydrogen (Reaction 2) followed by secondary, reductive amination of the resultant carbonyl to form the amine (Reaction 3). The latter step—reductive amination of a carbonyl—is usually subdivided into a sequence of nucleophilic

addition of ammonia to the carbonyl to form an imine (Reaction 4) and hydrogenation of the imine intermediate to form the amine (Reaction 5).^{10,27,37,41} Further, it is generally agreed that dehydrogenation of the alcohol controls the overall rate of alcohol amination.⁸ That said, it is debatable whether primary amines are truly sequential products during alcohol amination as implied by the borrowing hydrogen mechanism. It is unlikely that ammonia and simple carbonyls formed by alcohol dehydrogenation react homogeneously to form imines under typical reaction conditions.⁴² Moreover, there is no compelling evidence that producing an amine from an alcohol

requires the intermediate formation and secondary activation of bulk (i.e., non-surface) carbonyls or imines. We propose that the mechanistic interpretation presented by Baiker in describing alcohol amination over Cu seems more plausible. It suggests that aminations of alcohols and reductive aminations of carbonyl compounds both proceed through a common surface intermediate.⁵² A consequence of this mechanism is that amines can form through both primary pathways (direct alcohol amination) and secondary pathways (reductive carbonyl amination) during alcohol amination.

Numerous reports detail alcohol aminations over soluble metal complexes^{53–55} and supported metal clusters (Ni, Cu, Pt, Pd, Rh, Ru, Co). 56-63 Across all systems, extant challenges include selectivity control; preventing sequential alkylation of the primary amine product to form secondary and tertiary amines; catalyst deactivation; and a limited substrate scope with ammonia. 41,57,58,62,64 Acknowledging the mechanistic insights gained through the study of molecular catalysts, we restrict our consideration to supported metals. Specifically, we aim to understand relationships between operating conditions, activity, selectivity, and stability during the amination of secondary alcohols with ammonia over Ru/SiO₂, and we emphasize rational operation of catalytic reactors to maximize primary amine yields. We have chosen Ru because it is active for the interconversion of alcohols and carbonyls. 65-77 This suggests high rates of alcohol amination, which aligns with many prior demonstrations of alcohol amination over Ru. 7,8,10,37,50,78-81 Moreover, Ru-based catalysts are reportedly more selective to primary amines than those based on Pd or Pt.82 In addition to elucidating strategies for selectivity control, we extend substrate scope from monofunctional, aliphatic secondary alcohols (e.g., isopropanol, 2-butanol, cyclohexanol) to heterocyclic secondary alcohols (hydroxytetrahydrofurans and hydroxytetrahydropyrans) that can potentially be sourced from biomass.83-89 The latter classes are intriguing substrates as their amination produces

bifunctional heterocycles (aminotetrahydrofurans and aminotetrahydropyrans), which may have unique applications as platform molecules. Finally, we examine yields of primary amines using both packed bed reactors (gas-phase) and batch reactors (liquid phase), and we consider the potential feasibility of a hydrogen-free approach for alcohol amination over Ru/SiO₂.

Silica (481 m²/g, Sigma Aldrich) and ruthenium (III) chloride hexahydrate (35–40% Ru, Acros

Materials & methods

Reagents

Organics) were used in catalyst synthesis. Gases used in catalyst pretreatment, catalyst characterization, operation of flow reactors, and instrument calibration were H₂ (99.999%, Airgas), He (99.999%, Airgas), NH₃ (Anhydrous, Airgas), N₂ (99.999%, Airgas), air (zero-grade, Airgas), CO (99.99% Airgas), O₂/He (1% O₂, 1% Ar, 98% He, Airgas), propylene (1% propylene, 1% Ar, 98% He, Airgas), and propane (1% propane, 1% Ar, 98% He, Airgas). Deionized water was purified in house by reverse osmosis, UV oxidation, and ion exchange to achieve a resistivity \geq $18.2 \text{ M}\Omega$ cm. Batch experiments were performed using n-decane (99%, Alfa Aesar) as a solvent. We consider the amination of various aliphatic and heterocyclic secondary alcohols, and amination products in each case are primary amines (Figure 1). We further propose that primary amines can be produced either through direct amination of the alcohol (Reaction 1) or through sequential dehydrogenation of the alcohol (Reaction 2) followed by reductive amination of the resultant ketone (Reaction 3). Imines (R₂C=NH) are purported intermediates during ketone amination over Ru (Reactions 4 and 5); however, we were unable to confirm their formation experimentally. This is consistent with imine formation being, in general, thermodynamically unfavorable. For example, at 298K, the reaction between formaldehyde and ammonia to form methanimine and water is endergonic ($\Delta G^{\circ} \approx 20 \text{ kJ mol}^{-1}$), whereas the subsequent reaction between methanimine and

hydrogen to form an methanamine is strongly exergonic ($\Delta G^{\circ} \approx -90 \text{ kJ mol}^{-1}$); as such, one anticipates trace imine concentrations under dihydrogen, even if ketone amination necessarily proceeds through an imine intermediate. 90,91 Alcohols, ketones, and primary amines were therefore the only observable products in each amination scheme, so each amination experiment involved the purchase of three reagents. These are sorted by carbon number in Table 1. Alcohols were used as amination substrates; alcohols, ketones, and amines were used in calibration of gaschromatographs.

Table 1: List of reagents and calibration standards

Chemical	Carbon Atoms	Purity (%)	Manufacturer
2-propanol (isopropanol)	3	99.9	Acros
2-propanone (acetone)	3	99+	Acros
2-aminopropane (isopropylamine)	3	99	Acros
2-butanol	4	99	Alfa Aesar
2-butanone	4	99+	Acros
2-aminobutane	4	99	Acros
3-hydroxytetrahydrofuran	4	98	Oakwood
3-oxotetrahydrofuran	4	95	Alfa Aesar
3-aminotetrahydrofuran	4	>97	TCI
2-pentanol	5	98	Acros
2-pentanone	5	99	Acros
2-aminopentane	5	>97	TCI
cyclopentanol	5	99	Acros
cyclopentanone	5	99+	Acros
cyclopentylamine	5	99+	Acros
4-hydroxytetrahydropyran	5	98	Oakwood
4-oxotetrahydropyran	5	98	Oakwood
4-aminotetrahydropyran	5	98	Oakwood
cyclohexanol	6	98	Acros
cyclohexanone	6	99.8	Acros
cyclohexylamine	6	99	Acros
2-octanol	8	98	Alfa Aesar
2-octanone	8	99+	Acros
2-aminooctane	8	>98	TCI

Catalyst synthesis and characterization

Ru/SiO₂ catalysts were prepared by incipient wetness impregnation of aqueous ruthenium (III) chloride hexahydrate into amorphous SiO_2 . Ru concentrations were adjusted to achieve targeted metal loadings in different catalyst samples. Prior to impregnation, silica was crushed and graded using a standard set of sieves. Particles between $45 - 90 \mu m$ were retained and calcined under

flowing air (100 ml min⁻¹, 450°C, 3 K min⁻¹, 4 h). Precursor solutions were then added dropwise to calcined silica at a loading of 1.6 mL g⁻¹. Samples were next held in ambient air for 12 hours, dried in an oven for 2 hours (90°C), reduced under H₂ flow (100 ml min⁻¹, 400°C, 3 K min⁻¹, 4 h), and cooled to ambient temperature under H₂. The cell was then purged with He (100 ml min⁻¹), and catalysts were passivated at ambient temperature under 1% O₂/He (50 ml min⁻¹, 30 min). Surface areas were determined by BET analysis of N₂ adsorption isotherms at 77 K (Micromeritics ASAP 2020). Prior to N₂ dosing, samples were outgassed under vacuum (6 h, 523 K).

Ru surface site densities were estimated using CO chemisorption at 308 K (Micromeritics ASAP 2020).65,93 Before CO dosing, samples were reduced in flowing H₂ (3 h, 673 K, 3 K min⁻¹), evacuated at 673 K for 1h, and cooled to 308 K under vacuum. Next, a CO adsorption isotherm was measured at 308K. The sample was then evacuated at 308K to remove physisorbed CO, and a second isotherm was collected at 308K. The difference in uptake between the two isotherms gives the quantity of chemisorbed CO, which we take as equivalent to the number of accessible Ru surface atoms. We should note that there is no clear consensus on the adsorption stoichiometry for CO on Ru. 94,95 That said, we have generally observed that carbonyl hydrogenation rates over zerovalent Ru scale linearly with CO uptake, 65-67 suggesting that an adsorption stoichiometry of 1:1 is reasonable. This aligns with observations by Davydov and Bell, who report linearly bound CO (as opposed to polycarbonyl species) on fully reduced Ru, and it roughly agrees with the works of Gonzalez, who suggests that, on average, the adsorption stoichiometry for CO on Ru is is \approx 1.2. 96-98 A detailed consideration of structure sensitivity and particle size effects is outside the scope of this work, and we take CO uptake as a rough, but adequate proxy for the accessible Ru surface area in this system. The average Ru particle size was estimated using Equation 1, which assumes hemispherical clusters.

$$d_p = \frac{6}{S_{Ru}\rho_{Ru}} \tag{1}$$

 S_{Ru} is the ratio of Ru surface area to the total mass of Ru deposited on the support during synthesis. Ru surface area was estimated from irreversible CO uptake by assuming that the area of a single Ru atom is 6.14 Å². The density of Ru (ρ_{Ru}) is 12.3 g cm⁻³.

Catalytic activity testing

Vapor-phase reactions were carried out in a 6.5" packed bed reactor (0.5" OD, 316 stainless steel) at temperatures between 407K and 448K and pressures from 1.0 bar to 4.6 bar. Reactor temperature was controlled at the outer wall using a Type K thermocouple and a PID temperature controller (LOVE 16A 3010). Reactor pressure was adjusted using a back pressure regulator (Tescom). The catalyst bed was supported at the middle of the reactor using quartz wool. Quartz chips were added upstream of the bed, and an inline thermocouple (Type K) was placed downstream to monitor internal temperature. Prior to reagent introduction, the bed was reduced in situ under H₂ (100 ml min⁻¹, 400°C, 3 °C min⁻¹, 4 h) and then cooled to reaction temperature. Gas feeds (H₂, NH₃, He) were regulated using mass flow controllers (Brooks SLA5850). Liquids were introduced into a heated vaporization chamber using a syringe pump (Cole-Parmer series 100) and mixed with gas feeds upstream of the catalyst bed. Effluent gases from the packed bed were transferred downstream for analysis through heat-traced, stainless-steel tubing. An inline gas chromatograph (HP 5890 Series II) was used for quantitative analysis of the effluent gas composition. Species were resolved using an Agilent CP-WAX column (0.32 mm x 25 m) and quantified using an FID detector.

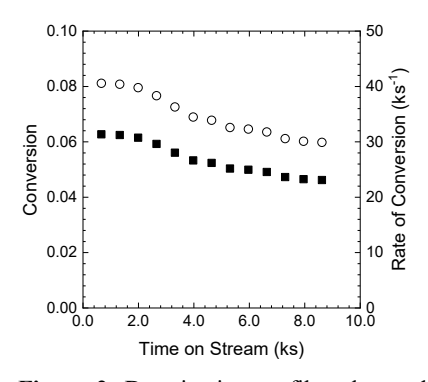


Figure 2: Deactivation profiles observed during reactor startup over Ru/SiO₂-A (0.6 wt% Ru); conversion (\blacksquare), rate of conversion (\bigcirc). pIPA = 0.005 bar; pNH₃ = 0.40 bar, pH₂ = 0.60 bar, T = 433K. Carbon balances for all data points illustrated here closed within 5%.

Packed bed experiments were initiated by allowing the reactor to reach steady state under isopropanol ($5.3 \times 10^{-3} - 0.022$ bar), NH₃ (0.20 - 0.40 bar), H₂ (0.10 - 0.50 bar), and He (balance); as illustrated in Figure 2, this requires 9 - 10 ks on stream (≈ 3 h). During the approach to steady state at low isopropanol conversion (< 10%), we observe a 20 – 30% decrease in isopropanol conversion rates; thereafter, activity and selectivity stabilize. To probe the impacts of various operating conditions, we recorded the initial steady state

characteristics to establish a benchmark reference condition. Then, we introduced perturbations in temperature, species partial pressure, contact time, and/or alcohol identity. After the perturbation, the system was allowed to reach a new steady state, and metrics were again recorded. Finally, the system was returned to startup conditions, which allowed us to detect and correct for changes in baseline catalyst activity (deactivation or regeneration) induced by the perturbation. Where rate data are reported, they are corrected to the initial "reference" steady state measured at the start of a specific experiment. They are not corrected to an absolute rate at zero time on stream. This is adequate here because we primarily discuss relative changes in reaction rate in response to perturbations in operating conditions.

For packed bed experiments, carbon balances closed to \pm 10%, and we define conversion, selectivity, and yield based on carbon in products (Equations 2 – 4). $F_{i,f}$ represents the feed molar flowrate of reactant i, F_j represents the effluent molar flowrate of product j, and N_C represents the number of carbon atoms in each species.

$$X_{i} = \frac{\sum_{j} N_{C,j} F_{j}}{N_{C,i} F_{i,f}} \tag{2}$$

$$S_j = \frac{N_{C,j} F_j}{\sum_j N_{C,j} F_j} \tag{3}$$

$$Y_j = \frac{N_{C,j} F_j}{N_{C,i} F_{i,f}} \tag{4}$$

Since we employ a range of Ru loadings and samples with different average cluster sizes, packed bed contact times (τ) are defined based on the feed molar flowrate of reactant and the total number of Ru surface sites in the catalyst bed as estimated by CO chemisorption (N_{Ru}).

$$\tau = \frac{N_{Ru}}{F_{i,f}} \tag{5}$$

We cannot claim a definitive analysis of particle size effects, but we see no evidence of significant structure sensitivity, suggesting that this is an appropriate definition of residence time. Similarly, we report the effluent flowrates of reaction products as site-time-yields, which are defined in Equation 6.

$$STY_j = \frac{F_j}{N_{Ru}} \tag{6}$$

Liquid-phase reactions were carried out in a magnetically stirred, home-built, stainless steel batch reactor with an internal volume of 60mL. The reactor was equipped with valves for gas introduction; a gas purge valve; a liquid sampling loop; a rupture disk; and a thermocouple port. It was heated externally using a band-heater. Reactor temperature was controlled at the external wall using a K-type thermocouple and a PID controller (LOVE, Series 16A). A typical batch reaction was conducted by adding catalyst, solvent, and alcohol to the vessel. It was then sealed and purged

under H₂ flow (85 ml min⁻¹, 10 min) at ambient temperature. Next, the pressures of ammonia and hydrogen were adjusted to 6.4 bar and 13.6 bar, respectively. Finally, the reactor was heated to the desired temperature, and samples were extracted periodically to track reaction progress. Recognizing that conversions and yields in a catalytic batch reactor reflect a convolution of reaction time, the initial quantity of reactant, and the number of active sites, we define a batch residence time as the product of reaction time (t) and the molar ratio of the number of Ru surface sites present in the reactor (N_{Ru}) to the initial quantity of alcohol added to the batch reactor (N_{ALC}). This definition is a molar analog to the batch residence time described by Baiker,⁵² and it allows us to account for variations in reactant quantity, mass loading, and Ru dispersion in batch experiments.

$$\tau = \frac{N_{Ru}t}{N_{ALC}} \tag{7}$$

Liquid-phase species concentrations were determined using a gas-chromatograph (HP 5890 Series II), which was equipped with a CP-WAX column (0.32 mm x 25 m) and an FID detector. Gas-phase products were not analyzed. Accounting for only liquid-phase carbon was adequate to ensure carbon balance closure (\pm 15%) at temperatures below 443K. Above 443K, we were only able to account for 70 - 80% of the feed carbon, especially at long residence times. Presumably, this is attributed to the formation of gas phase side-products, which are favored at elevated temperatures and not quantified in batch experiments. We thus avoid a detailed discussion of product selectivity and instead focus on yields of liquid-phase products (Equation 8). The yield for product j (Y_j) was calculated in molar units based on the total moles of product j collected (N_j) and the total quantity of alcohol reactant j added to the batch system ($N_{i,0}$) using.

$$Y_j = \frac{N_j}{N_{i,0}} \tag{8}$$

Diamine and triamine analogs of each alcohol in Table 1 are not commercially available; however, diisopropylamine (99+%, Acros) and triisopropylaime (97%, Oakwood) can be purchased to permit consideration of the sequential amination of isopropanol. Although we did not specifically examine correlations between operating conditions and sequential amination rates, we have found that during isopropanol amination (a) over Ru/SiO₂, (b) between 400 – 440K, and (c) under a large NH₃/H₂ excess, selectivity toward secondary and tertiary amines was below 10% at high conversion (> 70%) and typically below 1% at low conversion (< 30%). Maximum combined yields to diisopropylamine and triisopropylamine across all experiments were approximately 7% at isopropanol conversions approaching 100%, allowing us to categorize them as trace products. This is consistent with Bell's observation that excess ammonia strongly favors primary amine formation during 1-propanol amination over Ni-Hydroxyapatite at 423K.⁴² Aminations of other alcohols were always performed under similar conditions to minimize sequential amination. For this reason, secondary and tertiary amines were not generally quantified. Importantly, this did not prevent carbon balance closure, which supports trace formation of secondary and tertiary amines.

Computational methods

Non-periodic DFT calculations

Thermodynamic properties were estimated using the electronic structure program TURBOMOLE 7.5. $^{99-101}$ First, a geometry relaxation was performed at the DFT level of theory using the range-separated ω B97X-D functional to describe electron exchange and correlation effects. 102 Atoms were described by an all-electron basis-set of triple- ζ quality (TZVP). $^{103-105}$ Molecular structures were relaxed until the maximum magnitude of SCF energy change and gradients were less than

 1.0×10^{-8} and 1.0×10^{-4} au, respectively. A spherical m5 quadrature grid was used for numerical integrations. Auxiliary basis sets were used to approximate the Coulomb potential within the RI-J approximation to speed up the calculation. Next, vibrational frequencies were evaluated within the harmonic approximation using the *aoforce* module implemented in the TURBOMOLE package. Molecular thermodynamic functions (e.g., enthalpy and entropy) were then calculated assuming that the ideal gas approximation is valid and that all degrees of freedom are decoupled.

Planewave DFT calculations

Non-spin polarized plane-wave DFT calculations were performed using the Vienna Ab-initio Simulation Package (VASP 5.4.4). 110,111 A frozen-core, all-electron projector augmented wave (PAW) approach was used to describe electron-ion interactions. 112 The Perdew-Burke-Ernzerhof (PBE) functional 113,114 with Grimme's D3 dispersion correction 115 was used to treat exchange-correlation effects within the Generalized Gradient Approximation (GGA). Basis sets included wavefunctions with kinetic energy up to 420 eV. A convergence criterion of 1.0×10^{-7} eV was set for the electronic Self-Consistent Field (SCF) loops. Structures were considered relaxed when the maximum force on any atom was less than 0.01 eV/Å. Harris corrections based on the Harris-Foulkes formalism were applied to forces and stress tensors, 116,117 and total energy was corrected for dipole effects using a modified version of the Makov-Payne scheme. 118 The Brillouin zone was sampled using a Monkhorst-Pack 4 × 4 × 1 k-point grid. 119 First-order Methfessel-Paxton smearing ($\sigma = 0.10$ eV) was used to accelerate convergence of reciprocal space integrals with respect to the number of k-points. 120 Bulk lattice parameters for HCP-Ru were calculated to be $(a_{Ru} = 2.697$ Å, c/a = 1.582), which are in good agreement with experimental data ($a_{Ru} = 2.705$

Å, c/a = 1.582).¹²¹ Next, a Ru(0001) periodic surface model was constructed as a four-layered (4 × 4) supercell. The top two layers were allowed to relax during geometry optimization, while the bottom two layers were fixed to their bulk positions. A 15 Å vacuum gap was added along the surface normal to ensure that the charge density in this direction approaches zero. Harmonic vibrational frequencies were calculated using a numerical Hessian matrix using the tools implemented in the VTST package for VASP developed by Henkelman.^{122–124} We used the central-difference approximation for the Hessian computation, wherein the adsorbate atoms were displaced by 0.005 Å from their equilibrium positions.

Calculation of adsorption energy

The adsorption energy of a molecule (A) was calculated using Eq. (9), where E_{A+slab}^0 is the zero-point corrected (ZPE) ground-state energy of the slab-adsorbate complex, E_{slab} is the energy of a bare metal slab, and $E_{A(g)}^0$ is the ZPE corrected ground-state energy for gas-phase species. Endothermic binding energies referenced herein are the negative of the adsorption energy.

$$\Delta E_A^{ads,0} = E_{A+slab}^0 - E_{slab} - E_{A(g)}^0 \tag{9}$$

The magnitude of the ZPE corrections to the 0 K SCF energy was computed using Eq. (10). To partially overcome the limitation of DFT and the harmonic approximation in describing low-lying vibrational frequencies (ν_i), we assigned a cutoff value of 50 cm⁻¹ to any frequency that is smaller than 50 cm⁻¹.¹²⁵

$$ZPE = \frac{1}{2} \sum_{i} h \nu_i \tag{10}$$

Results & Discussion

Table 2 summarizes metal loading, surface area, CO uptake, fraction of exposed Ru atoms (CO:Ru), and average Ru cluster sizes (d_p) for the SiO₂ support and Ru/SiO₂ catalysts. To sample a large range of residence times and conversions, Ru/SiO₂ catalysts were synthesized at various metal loadings. Particle size heterogeneity is observed when varying metal loading from 0.6 wt% to 14.6 wt%; accordingly, CO uptake was used to correct for dispersion effects in defining contact times and site time yields.

Table 2: Physicochemical properties of Ru/SiO₂ catalysts

Sample	Metal Loading		BET Surface Area	CO uptake	CO:Ru	d_p
	wt %	μmol Ru/m² SiO ₂	$m^2 g^{-1}$	μmol g ⁻¹		nm
SiO ₂	0	0	481	-	-	
Ru/SiO2-A	0.6	0.124	467	18.0	0.31	4.4
Ru/SiO ₂ -B	1.5	0.313	520	62.0	0.41	3.2
Ru/SiO2-C	3.3	0.702	467	86.0	0.26	5.1
Ru/SiO ₂ -D	14.6	3.520	426	263	0.18	7.3

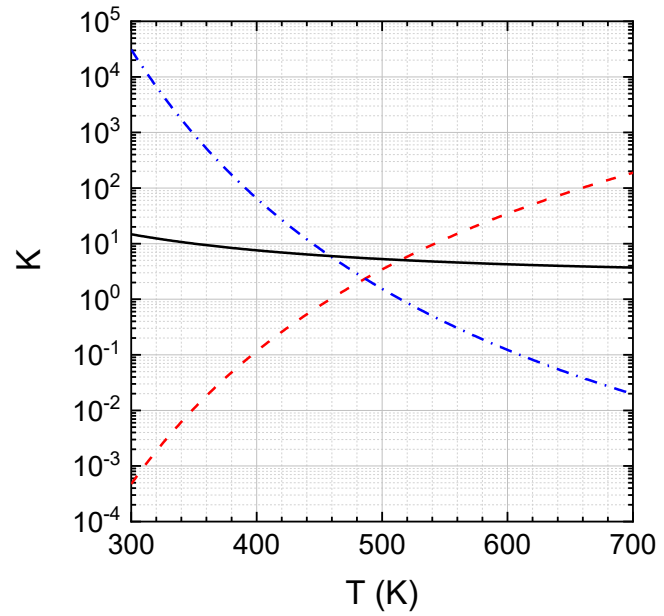


Figure 3: Equilibrium constants for isopropanol amination (----), isopropanol dehydrogenation (-----), and reductive amination of acetone (-----) as a function of temperature.

We begin with analysis of isopropanol amination, and we subsequently extend insights to the full set of secondary alcohols compiled in Table 1. Prior to an examination of site time yields, conversion, and product selectivity, we consider thermodynamic constraints on the three observable reactions outlined in Figure 1: direct amination of isopropanol (1), dehydrogenation of isopropanol (2), and

reductive amination of acetone (3). Equilibrium constants for each reaction are presented as a function of temperature in Figure 3.^{90,91} Isopropanol amination is marginally favorable and exothermic ($\Delta H^{\circ} \approx -7 \text{ kJ mol}^{-1}$, $\Delta S^{\circ} \approx -0.7 \text{ J mol}^{-1} \text{ K}^{-1}$), so its equilibrium constant decreases from

approximately 15 to 4 between 300K and 700K. Considering only the direct amination of isopropanol, equilibrium constants in this range mean that it is possible to obtain near-quantitative yields of isopropylamine during isopropanol amination, but it requires operating under excess ammonia (N_{NH3} : $N_{C3H8O} \approx 10$). If one instead considers a sequential amination pathway wherein acetone is formed as an intermediate, isopropanol dehydrogenation is endothermic and entropically favorable ($\Delta H \approx 55 \text{ kJ mol}^{-1}$, $\Delta S \approx 125 \text{ J mol}^{-1} \text{ K}^{-1}$); as such, isopropanol dehydrogenation transitions from an unfavorable equilibrium at 300K (K $\approx 5.0 \times 10^{-5}$) to a favorable equilibrium at 700K (K \approx 200). In contrast, acetone amination is exothermic and entropically unfavorable ($\Delta H \approx -65 \text{ kJ mol}^{-1}$, $\Delta S \approx -120 \text{ J mol}^{-1} \text{ K}^{-1}$). Therefore, acetone amination is favorable at 300K (K = 3.6 x 10^4), and it becomes unfavorable at 700K (K \approx 0.02). At the outset, it is unclear how thermodynamic constraints on isopropanol dehydrogenation and acetone amination will impact conversion and selectivity during isopropanol amination, but assuming all reactions are kinetically accessible, one anticipates a shift from amine-rich product distributions at low temperatures to ketone-rich product distributions at high temperatures. From another perspective, increasing reaction temperature will increase the demand for excess ammonia to drive higher equilibrium yields of primary amines. We further note that if isopropanol amination must proceed through acetone formation, it may be kinetically challenging to obtain high amine yields at low temperatures and under H₂ atmospheres. Under these conditions, isopropanol dehydrogenation is thermodynamically unfavorable, so one anticipates low acetone pressures and, presumably, rates of acetone amination. To ascertain the extent of thermodynamic control under a given set of experimental conditions, we subsequently report the reversibility for all reactions, z_i , observed at the reactor exit. 126 This is defined as the ratio of the reaction quotient, Q, to the equilibrium constant K for a specific reaction i, and we present it alongside rate, conversion, and

selectivity data. The reaction quotient is defined as a function of thermodynamic activities, a, and stoichiometric coefficients, v, for reacting species.¹²⁷

$$z_i = \frac{\prod_j a_j^{\nu_{i,j}}}{K_i} \tag{11}$$

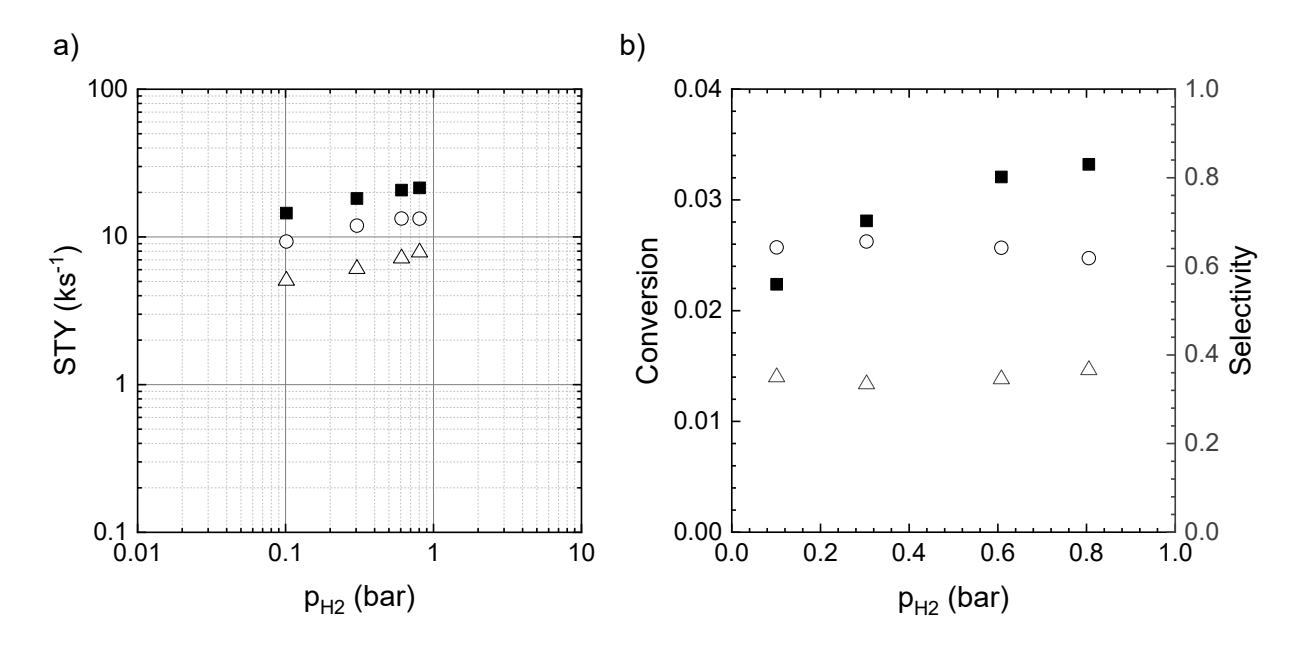


Figure 4: Dependence of (a) reaction rate and (b) conversion/selectivity on hydrogen partial pressure over Ru/SiO₂-A (0.6 wt% Ru). (\blacksquare) isopropanol conversion; (\bigcirc) isopropylamine formation; (\triangle) acetone formation. T = 433K, p_{OH} = 0.0053 bar, p_{NH3} = 0.20 bar, τ = 1.54s. For data illustrated here, we observed maximum reversibilities (z_i) well-below 1 for alcohol dehydrogenation (0.024), acetone amination (0.001), and isopropanol amination (1.0 × 10⁻⁶); this suggests observed trends are kinetic in origin.

Next, we consider trends in rate (site time yield), conversion, and product selectivity observed in response to changes in hydrogen partial pressure (Figure 4). Data were obtained under conditions where isopropanol conversions are below 0.03; reversibilities (z_i) for all reactions in Figure 1 are below 0.03; we see no evidence of strong product inhibition; and site time yields are weak functions of feed conversion. As such, the differential reactor approximation is reasonable, and one assumes that site time yields are a good approximation for turnover frequencies at feed conditions. The rate of isopropanol conversion has a slight positive order in H₂ (0.19 \pm 0.03), so increasing H₂ partial pressure from 0.1 bar to 0.8 bar at a residence time of 1.54 s causes a small

increase in isopropanol conversion (0.022 to 0.033). Individual site time yields to acetone and isopropylamine respond similarly to changes in H_2 partial pressure, respectively showing orders of 0.21 ± 0.08 and 0.18 ± 0.10 . Consequently, changing the H_2 partial pressure has no significant impact on product selectivity toward acetone (0.35 \pm 0.02) or isopropylamine (0.64 \pm 0.02). It is noteworthy that product selectivity is invariant in the conversion range from 0.02 - 0.03. Because there is a secondary pathway for isopropanol amination—namely reductive amination of acetone—selectivity may be sensitive to small changes in fractional conversion. Here, we observe no strong correlation between reaction extent and selectivity below about 5% conversion. This increases confidence that changes in selectivity at low conversion are attributable to variations in reaction rate(s) and not to variations in reaction extent.

Table 3: Summary of Isopropanol Amination as a function of hydrogen partial pressure at various conversion levels

Entry $\tau(s)$	- (-)	II (1)	C	Selectivity		Q/K		
	H ₂ (bar)	Conversion	Acetone	Isopropylamine	<i>Z</i> 1	Z 2	Z 3	
1	26.2	0.10	0.08	0.23	0.72	3.3×10^{-5}	0.005	0.017
2	26.2	0.20	0.11	0.24	0.71	6.2×10^{-5}	0.014	0.010
3	26.2	0.40	0.14	0.25	0.70	9.6×10^{-5}	0.039	0.006
4	26.2	0.60	0.15	0.25	0.71	1.2×10^{-4}	0.063	0.004
5	111	0.60	0.23	0.14	0.84	4.3 × 10 ⁻⁴	0.064	0.016
6	111	1.07	0.23	0.14	0.84	4.1×10^{-4}	0.109	0.009
7	111	1.78	0.22	0.14	0.84	3.8×10^{-4}	0.166	0.005
8	111	3.55	0.20	0.13	0.85	3.0×10^{-4}	0.265	0.003

 Ru/SiO_2 -B (1.5 wt% Ru), T = 433K, $p_{IPA} = 0.021$ bar, $p_{NH3} = 0.40$ bar

Table 3 extends trends in conversion, selectivity, and equilibrium position as a function of H_2 potential to higher partial pressures, longer residence times, and higher feed conversions. Results generally align with those observed by Murzin during the amination of 1-dodecanol over Ru/C at 423K.¹²⁹ Entries 1-4 summarize the impacts of H_2 partial pressures between 0.1 and 0.6 bar at $\tau = 26.2$ s (8 - 15% conversion), and Entries 5-8 summarize analogous results obtained at H_2 pressures between 0.6 and 3.55 bar at $\tau = 111$ s (20 - 23% conversion). At low H_2 pressures, we observe a minor increase in isopropanol conversion with increasing H_2 pressure, which is

consistent with the positive fractional H_2 order illustrated in Figure 3. That said, the kinetic benefit of increasing H_2 pressure diminishes above 1 bar, where conversion levels are insensitive to further increases in H_2 pressure. Similar to trends observed under differential conditions (Figure 4), acetone and isopropylamine selectivities are invariant with H_2 pressure within a small conversion range; however, substantially increasing fractional conversion benefits isopropylamine selectivity. Specifically, under differential conditions (0 - 5% conversion, Figure 4), we observe a 40:60 acetone:isopropylamine distribution. At 8 – 15% conversion (Table 3), the distribution shifts to 25:70 in favor of isopropylamine. Finally, the acetone:isopropylamine distribution is 14:84 between 20 – 23% conversion (Table 3). Although we cannot exclude a direct alcohol amination pathway, i.e., one that does not proceed through intermediate formation of vapor-phase acetone, a positive correlation between isopropanol conversion and isopropylamine selectivity is consistent with the formation of isopropylamine through secondary, reductive amination of acetone. This interpretation is reinforced by the observation that the increase in isopropylamine selectivity is accompanied by a commensurate decrease in acetone selectivity.

 H_2 does not appear in the overall reaction for isopropanol amination, so changing H_2 pressure does not impact the equilibrium position for isopropanol amination at a fixed conversion. In contrast, increasing H_2 pressure discourages isopropanol dehydrogenation, and it favors the reductive amination of acetone. For these reasons, despite roughly invariant conversion levels for a given contact time (8-15% at 26.2 s, 20-23% at 111 s), increasing the hydrogen partial pressure moves the dehydrogenation step closer to equilibrium $(z_2 \rightarrow 1)$, and it moves the reductive amination of acetone further from equilibrium $(z_3 \rightarrow 0)$. Overall, in this range of operating conditions and isopropanol conversions, the only reaction that begins to approach equilibrium is isopropanol dehydrogenation. Specifically, at a H_2 pressure of 3.55 bar and an isopropanol conversion of

roughly 20%, isopropanol dehydrogenation has a reversibility of $z_2 = 0.265$. In contrast, the amination of isopropanol ($z_1 = 3.0 \times 10^{-4}$) and acetone ($z_3 = 0.003$) remain far from equilibrium.

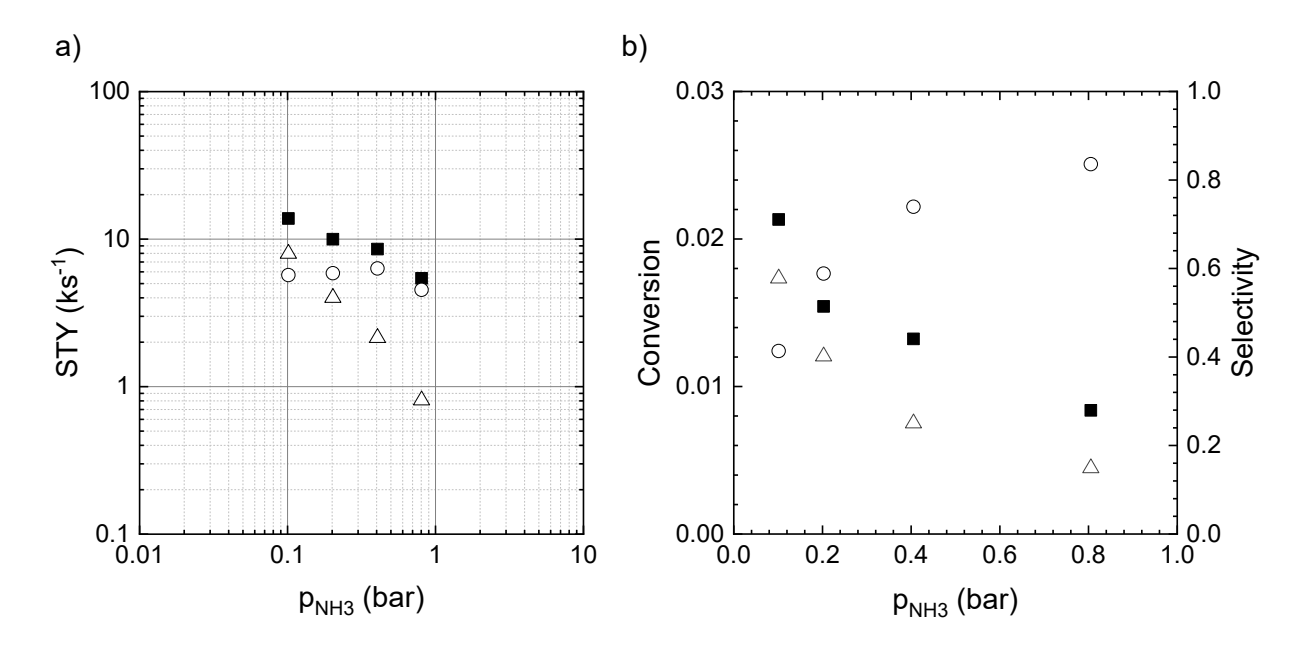


Figure 5: Dependence of (a) reaction rate and (b) conversion/selectivity on ammonia partial pressure over Ru/SiO₂-A (0.6 wt% Ru) at T = 433K, $p_{OH} = 5.3 \times 10^{-3}$ bar, $p_{H2} = 0.20$ bar, $\tau = 1.54$ s. (\blacksquare) isopropanol conversion; (\bigcirc) isopropylamine formation; (\triangle) acetone formation. For data illustrated here, we observed maximum reversibilities (z_i) well-below 1 for alcohol dehydrogenation (6.0×10^{-3}), acetone amination (2.7×10^{-4}), and isopropanol amination (6.6×10^{-7}); this suggests observed trends are kinetic in origin.

Next, we consider trends in rate, conversion, and selectivity as a function of ammonia partial pressure (Figure 5). Criteria used in justifying the differential reactor approximation when considering variations in H₂ pressure remain applicable; accordingly, we take site time yields to be reasonable approximations for turnover frequencies of isopropanol conversion, isopropanol dehydrogenation, and isopropanol amination at feed conditions. From Figure 5a, it is evident that increasing ammonia pressure between 0.1 and 1.0 bar inhibits isopropanol conversion. Interestingly, the decrease in isopropanol conversion rate arises entirely from a decrease in the dehydrogenation rate (acetone site time yield), whereas the amination rate (isopropylamine site

time yield) is largely unaffected. The latter is consistent with trends reported by Bell during the amination of 1-propanol over Ni/hydroxyapatite and Murzin in the amination of 1-decanol over Ru/C.^{42,129} We estimate apparent ammonia orders for the rate of isopropanol conversion (-0.43); the rate of isopropanol dehydrogenation (-1.08); and the rate of isopropanol amination (0.09). Consequently, increasing ammonia partial pressure from 0.1 bar to 0.8 bar benefits isopropylamine selectivity (0.41 – 0.84) at the expense of total isopropanol conversion. Conversion varies between 0.008 and 0.021 for the selectivity data reported here. Although this is a relatively small range, it is worth considering whether differences in selectivity arise due to changes in conversion, as the two can be strongly correlated for sequential reactions, even below 1% conversion. Here, we observe that selectivity trends run counter to expectations for primary and secondary reaction products. Specifically, selectivity toward acetone, a primary product of isopropanol dehydrogenation, increases with fractional conversion. Accordingly, we attribute the increase in isopropylamine selectivity with ammonia partial pressure to a suppression of ketone formation rates rather than to differences in fractional conversion.

Table 4: Summary of Isopropanol Amination as a function of ammonia partial pressure at various conversion levels

Entry $\tau(s)$	- (-)	NIII (h)	C	Selectivity		Q/K		
	NH ₃ (bar)	Conversion -	Acetone	Isopropylamine	<i>Z</i> 1	Z 2	Z 3	
1	26.2	0.10	0.16	0.60	0.36	1.4 x 10 ⁻⁴	0.108	0.003
2	26.2	0.20	0.14	0.43	0.54	1.2 x 10 ⁻⁴	0.069	0.004
3	26.2	0.40	0.13	0.28	0.70	8.2 x 10 ⁻⁵	0.040	0.050
4	26.2	0.60	0.12	0.21	0.77	5.1 x 10 ⁻⁵	0.027	0.005
5	111	0.60	0.21	0.11	0.88	2.4 x 10 ⁻⁴	0.027	0.021
6	111	1.07	0.18	0.07	0.92	1.1 x 10 ⁻⁴	0.016	0.016
7	111	1.78	0.15	0.06	0.94	4.2 x 10 ⁻⁵	0.010	0.010
8	111	3.55	0.10	0.05	0.95	8.4 x 10 ⁻⁶	0.005	0.004

 Ru/SiO_2 -B (1.5 wt% Ru), T = 433K, p_{IPA} = 0.021 bar, p_{H2} = 0.40 bar

Similar trends are observed under non-differential conditions (Table 4), where we consider conversion and selectivity during isopropanol amination at modest ammonia pressures (0.1 - 0.6) bar, Entries 1 - 4) and high ammonia pressures (0.6 - 3.55) bar, Entries 5 - 8). For a fixed residence

time, increasing ammonia pressure decreases isopropanol conversion while enhancing selectivity toward the primary amine. Under conditions summarized in Table 4, all reactions are far from equilibrium; as such, both impacts are attributed to kinetic effects. Specifically, increasing ammonia pressure inhibits the rate of isopropanol dehydrogenation without impacting the rate of amination. This manifests as a decrease in isopropanol conversion alongside an increase in isopropylamine selectivity. Although alcohol conversion remains low for the data presented in Table 4, it is noteworthy that one can drive primary amine selectivities well above 90% by operating in excess ammonia.

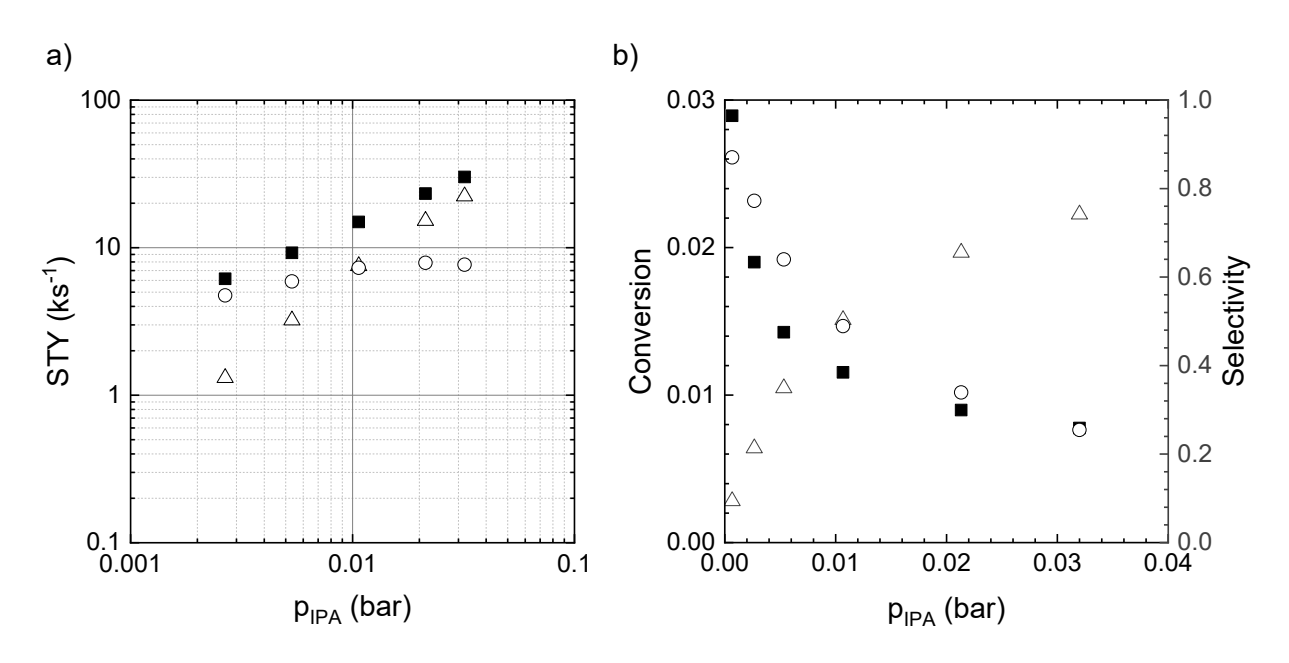


Figure 6: Dependence of (a) reaction rate and (b) conversion/selectivity on isopropanol partial pressure over Ru/SiO₂-A (0.6 wt% Ru) at T = 433K, pH₂ = 0.20 bar, pNH₃ = 0.20 bar, He balance, $\tau = 0.258$ - 12.4 s. (a) isopropanol conversion; (\circ) isopropylamine formation; (Δ) acetone formation. For data illustrated here, we observed maximum reversibilities (z_i) below 1 for alcohol dehydrogenation (2.9×10^{-3}), acetone amination (6.0×10^{-4}), and isopropanol amination (4.4×10^{-7}); this suggests observed trends are kinetic in origin.

Next, we consider trends in rate, conversion, and selectivity as a function of isopropanol partial pressure under differential conditions (Figure 6). The rate of isopropanol conversion has a

relatively strong response to changes in isopropanol pressure, exhibiting an apparent reaction order of 0.66 ± 0.02 ; however, this is a convolution of very different responses in the rates of dehydrogenation and amination. Changes in the acetone STY (Figure 6a) reveal that isopropanol dehydrogenation has a roughly first order dependence on isopropanol partial pressure (1.20 ± 0.09) . In contrast, changes in the isopropylamine STY suggest that isopropanol amination has a small, positive fractional order dependence on isopropanol pressure (0.34 \pm 0.17). This is consistent with trends observed during 1-propanol amination over Ni. 42 The fact that isopropanol dehydrogenation is significantly higher order in isopropanol (than isopropanol amination) results in a substantial increase in acetone selectivity with increasing isopropanol partial pressure (Figure 6b). Selectivity to isopropylamine increases with fractional conversion in this data set, which aligns with expectations for the formation of isopropylamine through a secondary pathway. That said, selectivity trends between fractional conversions of 0.01 – 0.03 observed when varying H₂ and NH₃ pressures suggest a weak correlation between conversion and selectivity in this range. We thus attribute the change in selectivity to differences in the isopropanol order for isopropanol dehydrogenation and isopropanol amination.

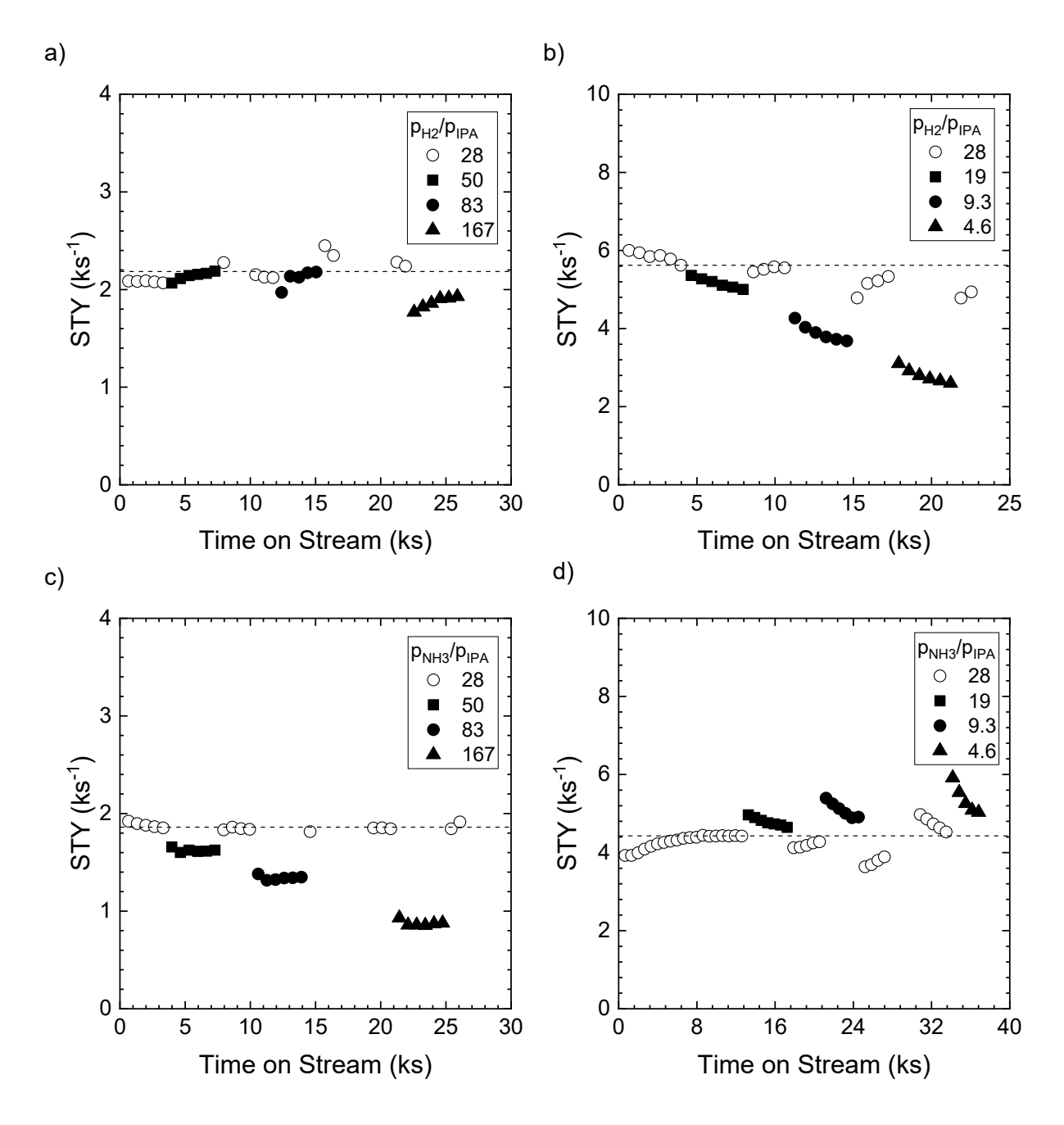


Figure 7. Rates of isopropanol conversion as a function of time on stream with variation in H_2 and NH_3 partial pressures over Ru/SiO_2 -B (1.5 wt% Ru) at T = 433K, $p_{IPA} = 0.021$ bar, and t = 26.2 s. Figure 7a: $p_{NH3} = 0.40$ bar, $p_{H2} = 0.60$ bar (\circ), 1.07 bar (\bullet), and 3.55 bar (\triangle). Figure 7b: $p_{NH3} = 0.40$ bar, $p_{H2} = 0.60$ bar (\circ), 0.40 bar (\bullet), 0.20 bar (\bullet), and 0.10 bar (\triangle). Figure 7c: $p_{H2} = 0.40$ bar, $p_{NH3} = 0.60$ bar (\circ), 1.07 bar (\bullet), 1.77 bar (\bullet), and 3.55 bar (\triangle). Figure 7d: $p_{H2} = 0.40$ bar, $p_{NH3} = 0.60$ bar (\circ), 0.40 bar (\bullet), 0.20 bar (\bullet), and 0.10 bar (\triangle). Dashed lines indicate the average rate measured at the startup/reference condition.

In addition to affecting intrinsic rates of dehydrogenation and amination, variations in species partial pressure also impact the baseline activity of Ru/SiO₂. To illustrate these effects, we present rates of isopropanol conversion as a function of time on stream in response to variations in H₂

pressure and NH₃ pressure (Figure 7). In general, we observe minimal catalyst deactivation under a large excess of H₂ and/or NH₃ (Figures 7a and 7c), whereas perturbations that decrease the ratio of H₂:isopropanol or NH₃:isopropanol below ≈ 20 induce deactivation (Figures 7b and 7d). Reversing the change back to excess H₂ or NH₃ restores the baseline activity of the catalyst. We cannot determine the precise mechanism of deactivation from the data presented, but one assumes that H₂- and NH₃-rich environments are sufficiently reducing to either maintain zerovalent Ru surface sites or to prevent the accumulation of hydrogen-deficient carbon deposits (i.e., coke).

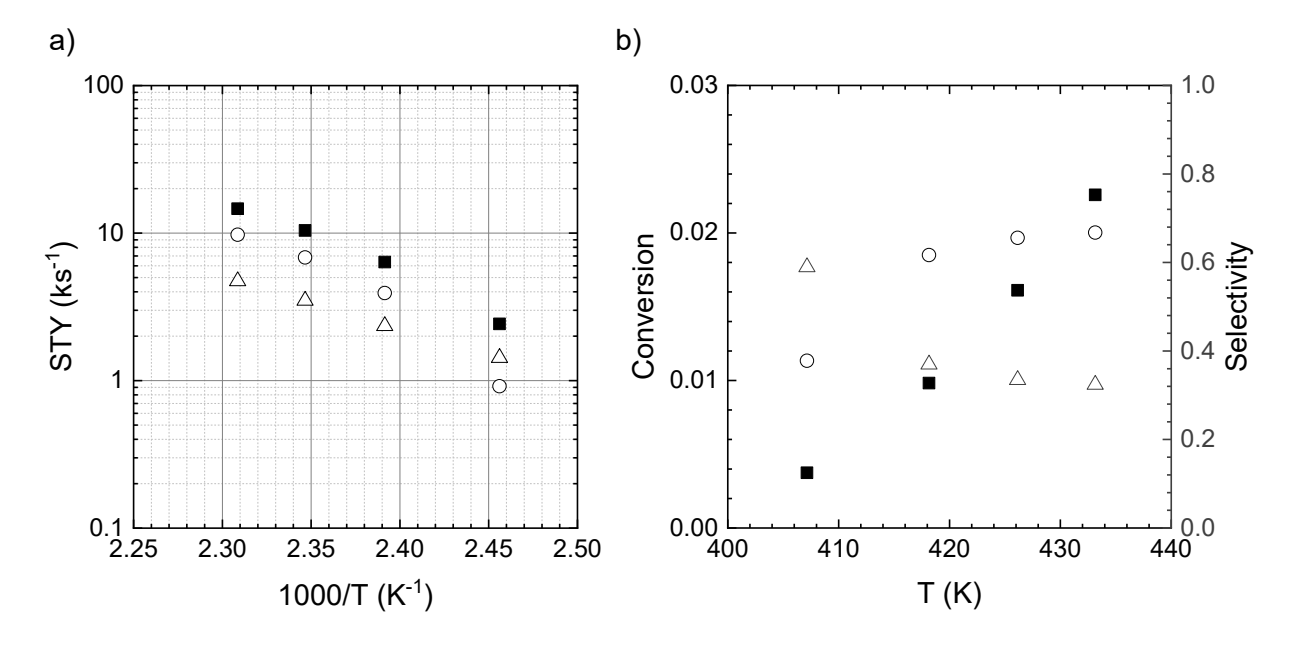


Figure 8. Dependence of (a) reaction rate and (b) conversion/selectivity on temperature over Ru/SiO₂-A (0.6 wt% Ru) at p_{OH} = 5.0×10^{-3} bar, p_{H2} = 0.20 bar, p_{NH3} = 0.20 bar, He balance, $\tau = 1.54$ s. (\blacksquare) isopropanol conversion; (\circ) isopropylamine formation; (\circ) acetone formation. For data illustrated here, we observed maximum reversibilities (z_i) below 1 for alcohol dehydrogenation (3.6 x 10^{-4}), acetone amination (6.0 x 10^{-4}), and isopropanol amination (9.3 x 10^{-7}); this suggests observed trends are kinetic in origin.

Next, we consider the influences of temperature on rate, conversion, and selectivity under differential conditions (Figure 8). Rates of isopropanol conversion, acetone formation, and isopropylamine formation all increase with temperature, albeit with different apparent barriers. The overall barrier for isopropanol conversion is 100 ± 36 kJ mol⁻¹, whereas respective barriers

for acetone and isopropylamine formation are 68 ± 5.6 kJ mol⁻¹ and 134 ± 82 kJ mol⁻¹. As such, temperature has a strong impact on product selectivity, with increasing temperature favoring amination. That said, there is a ceiling on leveraging temperature to improve amine selectivity as acetone becomes the thermodynamic product between 500 and 600K (Figure 3).

Thus far, we have observed good selectivity to acetone and isopropylamine at short residence times and low isopropanol conversion. Further, a thermodynamic analysis of the isopropanol amination network suggests that isopropylamine yields in excess of 95% are attainable as long as reactors operate below approximately 500K in excess ammonia. In theory, realizing these yields only requires increasing residence times to consume intermediate acetone by reductive amination; however, this neglects consideration of mitigating factors that may also arise at longer residence times. For example, the accumulation of strongly bound products or spectators might inhibit reaction rates, making it difficult to achieve high conversions in feasible residence times. Alternatively, side reactions may become problematic at longer residence times, which can limit isopropylamine yields. With this mind, we consider the impacts of increasing residence time at an isopropanol pressure of 0.021 bar, a H₂ pressure of 0.60 bar, an ammonia pressure of 0.40 bar, and reaction temperatures from 407 – 448K.

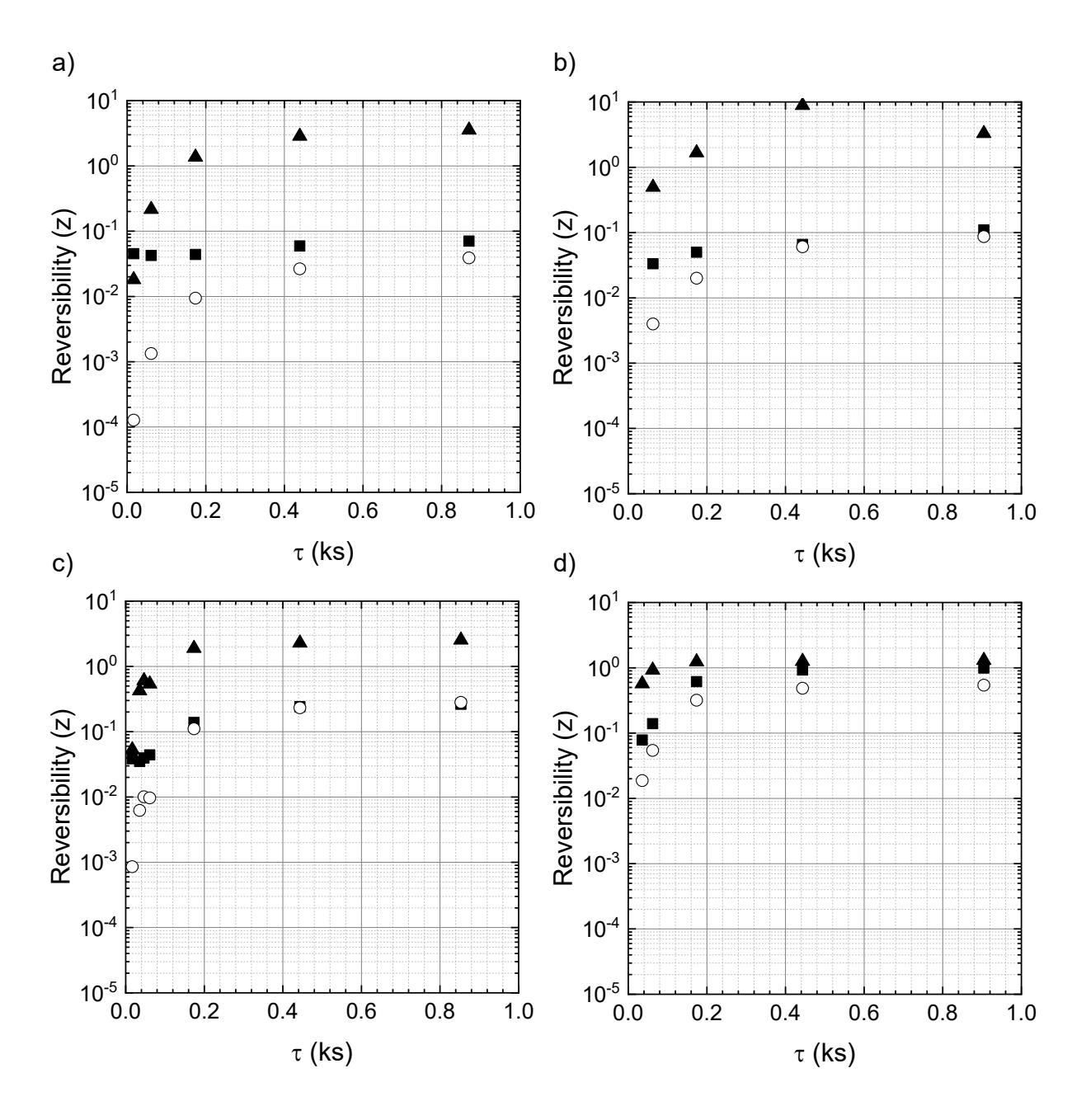


Figure 9. Reversibilities for isopropanol amination (z_1, \circ) , isopropanol dehydrogenation (z_2, \blacksquare) , and acetone amination (z_3, \triangle) as a function of residence time over Ru/SiO₂-C (3.3 wt% Ru) at pOH = 0.021 bar, pH₂ = 0.60 bar, pNH₃ = 0.40 bar and a) 407K, b) 418K, c) 433K, and d) 448K.

Figure 9 summarizes the approach to chemical equilibrium for macroscopically observable reactions as a function of residence time at 407K, 418K, 433K, and 448K. Imprecision in experimental determination of reaction quotients notwithstanding (e.g., acetone partial pressures

approach zero under many experimental conditions, decreasing confidence in z_2 and z_3), we find that acetone:isopropylamine (z_3) distributions reach equilibrium quickly compared to isopropanol:isopropylamine (z_1) and isopropanol:acetone (z_2). The full distributions of isopropanol, acetone, and isopropylamine approach chemical equilibrium only at elevated temperatures (448K) and residence times near 1.0 ks. These observations suggest that acetone amination is facile relative to isopropanol dehydrogenation and/or isopropanol amination, which is consistent with the prevailing view that the rate of α -hydrogen abstraction from the alcohol controls the rate of alcohol amination.⁸

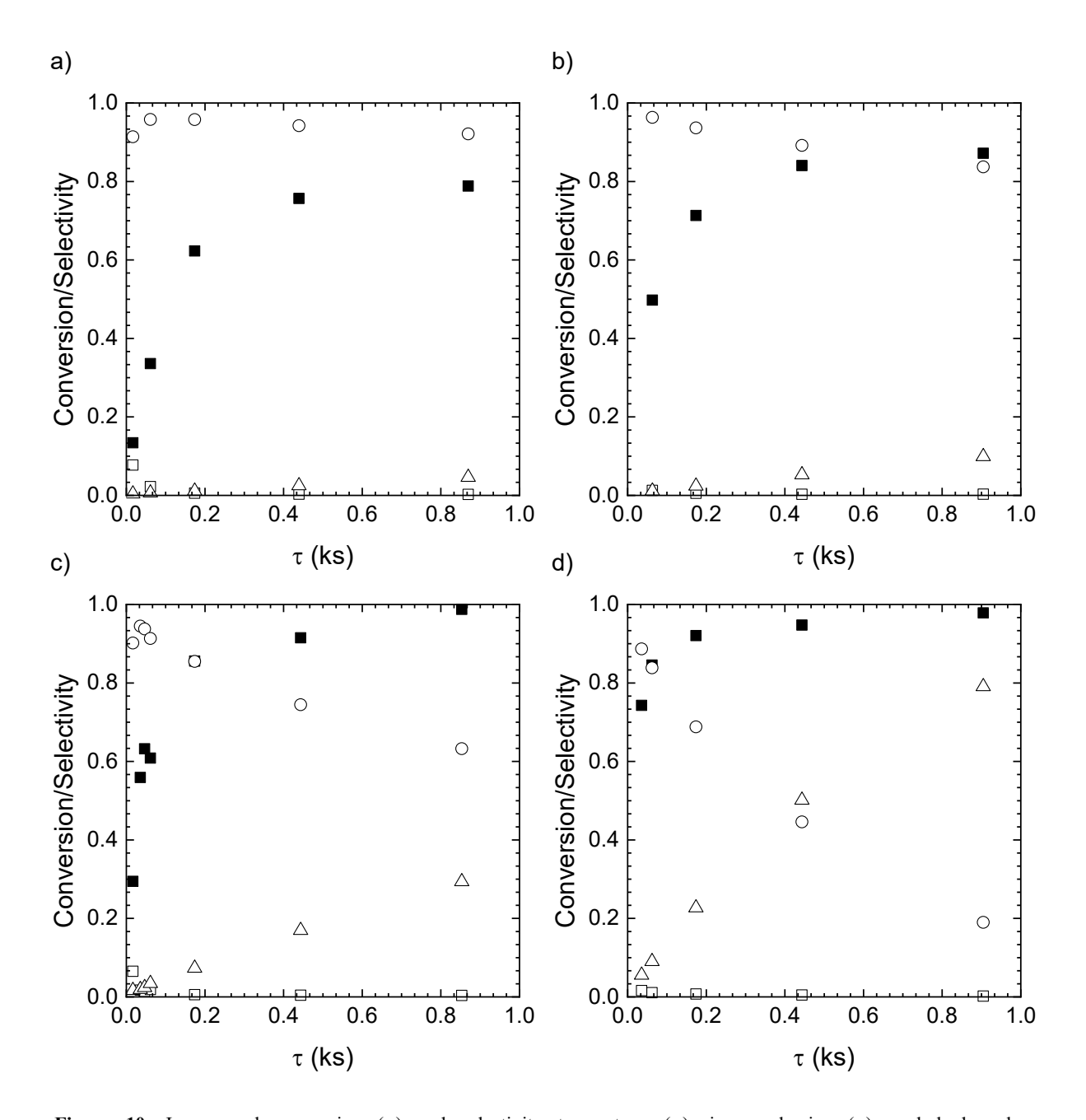


Figure 10. Isopropanol conversion (\blacksquare) and selectivity to acetone (\square), isopropylamine (\circ), and hydrocarbons (propane/propylene) (Δ) as a function of contact time during isopropanol amination over Ru/SiO₂-C (3.3 wt% Ru) at pOH = 0.021 bar, pH₂ = 0.60 bar, pNH₃ = 0.40 bar and a) 407K, b) 418K, c) 433K, and d) 448K.

Figure 10 summarizes conversions and selectivities observed with increasing residence time at 407K, 418K, 433K, and 448K. Data are taken from experiments used in generating approach to equilibrium profiles (Figure 9), so they provide a complementary view of reaction progress. In all cases, one observes minimal acetone formation. It is present only in significant quantities at short

residence times (< 0.1 ks), whereafter its partial pressure approaches zero. This is consistent with acetone being a reactive primary product of isopropanol dehydrogenation. Specifically, acetone is a primary product that is susceptible to rapid, secondary reductive amination. It is further consistent with acetone formation being thermodynamically unfavorable relative to both isopropanol and isopropylamine under these conditions. Across all temperatures, we observe high selectivities to isopropylamine at intermediate residence times (0 - 0.2 ks), whereas longer residence times favor the formation of C_3 hydrocarbons (propane, propylene). Selectivity toward C_3 hydrocarbons is temperature sensitive, with higher temperatures favoring hydrocarbon formation; as such, increasing reaction temperature shifts the onset of hydrocarbon formation to shorter residence times.

One can envision two plausible pathways for hydrocarbon formation in this system. One is dehydration of isopropanol (primary reaction),⁴⁷ and the other is deamination of isopropylamine (sequential reaction).⁴⁹ We observe no selectivity toward C₃ hydrocarbons in the zero-conversion limit; rather, hydrocarbons are observed only as isopropanol conversions increase above 50% and isopropylamine partial pressures become significant. Moreover, one observes similar hydrocarbon selectivities at equal isopropanol conversions regardless of temperature, i.e., hydrocarbon selectivity appears to be a stronger function of conversion than it does reaction temperature. For these reasons, one concludes that hydrocarbon formation arises not through primary dehydration or hydrogenolysis of isopropanol, but through the sequential deamination of isopropylamine. From a practical standpoint, high temperatures are attractive as they require minimal residence time to achieve high isopropanol conversions (< 1 ks); however, this must be balanced with the loss of isopropylamine selectivity arising from sequential deamination. One can minimize the extent of deamination by varying contact time, with optima depending on the reaction temperature. For

example, at 448K, isopropanol conversion exceeds 80% above 0.1ks, but selectivity toward isopropylamine decreases from \approx 90% at 0.1ks to \approx 20% at 1.0 ks, with the balance going to C₃ hydrocarbons. In contrast, one can maintain good selectivity toward isopropylamine at 407K, but contact times above 1.0ks are required to exceed 80% conversion. In general, we find a good compromise of activity and selectivity at 433K, where we observe 70 - 80% yields of isopropylamine at contact times of roughly 0.2 ks (Figure 11).

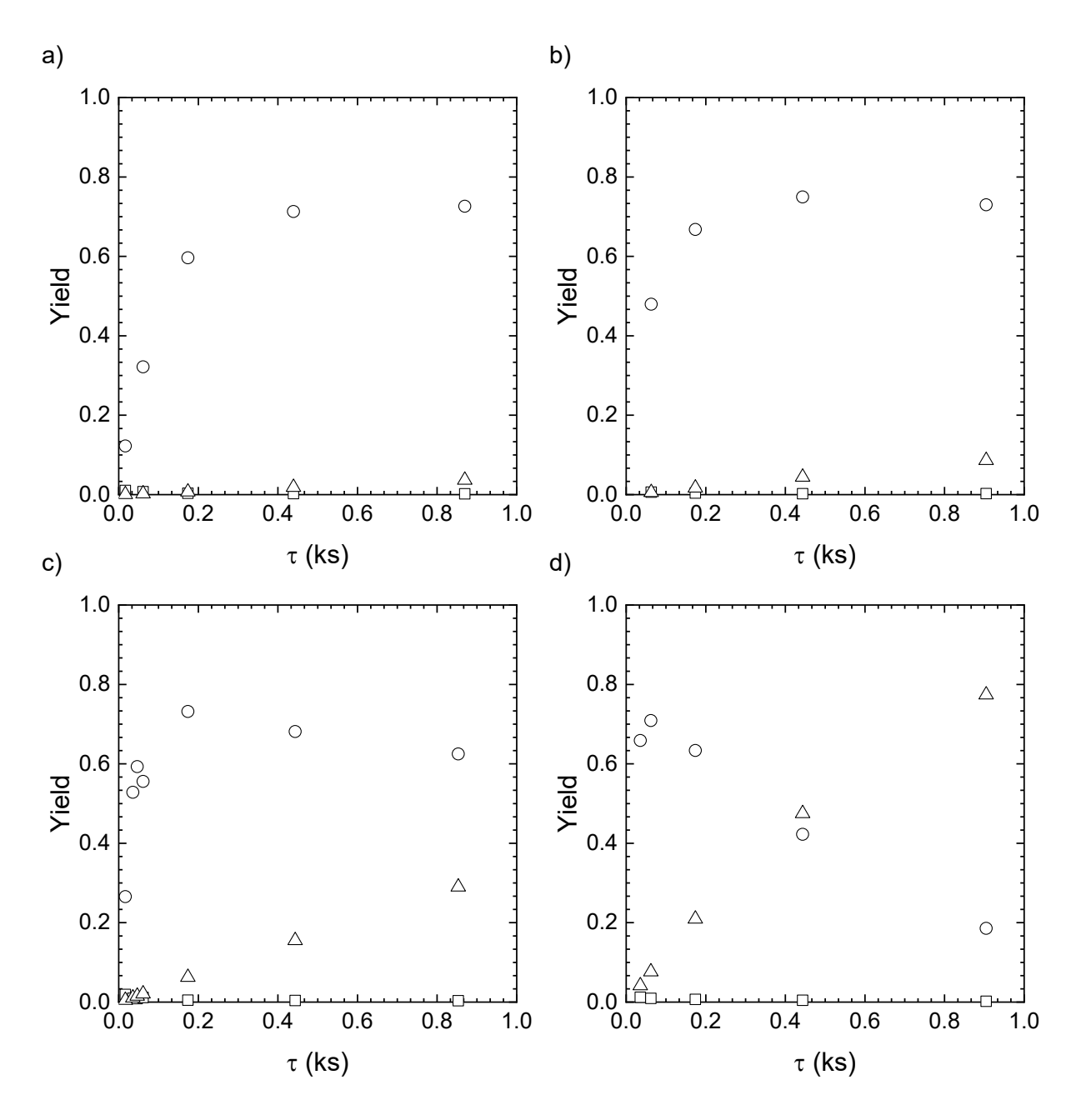


Figure 11. Yields to acetone, (\square), isopropylamine (\circ), and propane/propylene (Δ) observed as a function of contact time during isopropanol amination at a) 407K, b) 418K, c) 433K, and d) 448K. Ru/SiO₂-C (3.3 wt% Ru), pOH = 0.021 bar, pH₂ = 0.60 bar, pNH₃ = 0.40 bar.

Having identified an optimal range of temperatures (418 - 433K), residence times (0.1 - 0.3ks), and feed partial pressures ($p_{OH} = 0.021$ bar, $p_{NH3} = 0.40$ bar, $p_{H2} = 0.60$ bar), we consider an expansion of substrate scope to other secondary alcohols, including heterocyclic alcohols. The significance of the latter is that heterocyclic alcohols, namely hydroxytetrahydrofurans and

hydroxytetrahydropyrans, can potentially be sourced from biomass.^{83–89} This may open the door to bio-based platform chemicals that have multiple heteroatoms; as such, they are intriguing substrates for amination. To allow for rational control of residence times with substrate variation, we benchmarked amination rates for each of the secondary alcohols listed in Table 1. Experiments were carried out at 433K using reduced alcohol pressures ($p_{OH} = 0.0013$ bar) to facilitate vaporization of 2-octanol, 3-hydroxytetrahydrofuran (3-OH-THF), and 4-hydroxytetrahydropyran (4-OH-THP). NH₃ and H₂ pressures were maintained at a 150:1 excess relative to the alcohol to minimize deactivation and to favor amine formation at equilibrium. Data were obtained under differential conditions, and we report all rates normalized to that of 2-pentanol, which has the largest amination rate under the above-described conditions. Results are summarized in Figure 12. For monofunctional secondary alcohols, amination rates are relatively insensitive to structure/molecular weight. Specifically, 2-butanol (0.96), cyclohexanol (0.88), isopropanol (0.77), cyclopentanol (0.69), and 2-octanol (0.58) all display amination rates that are within a factor of two of 2-pentanol. This suggests that good primary amine yields should be attainable at similar contact times for all linear and cyclic monofunctional secondary alcohols. In contrast, heterocyclic secondary alcohols, namely 4-OH-THP (0.29) and 3-OH-THF (0.17), have 3- to 10-fold lower amination rates than 2-pentanol, suggesting a large increase in residence time will be necessary to achieve appreciable yields of their corresponding primary amines.

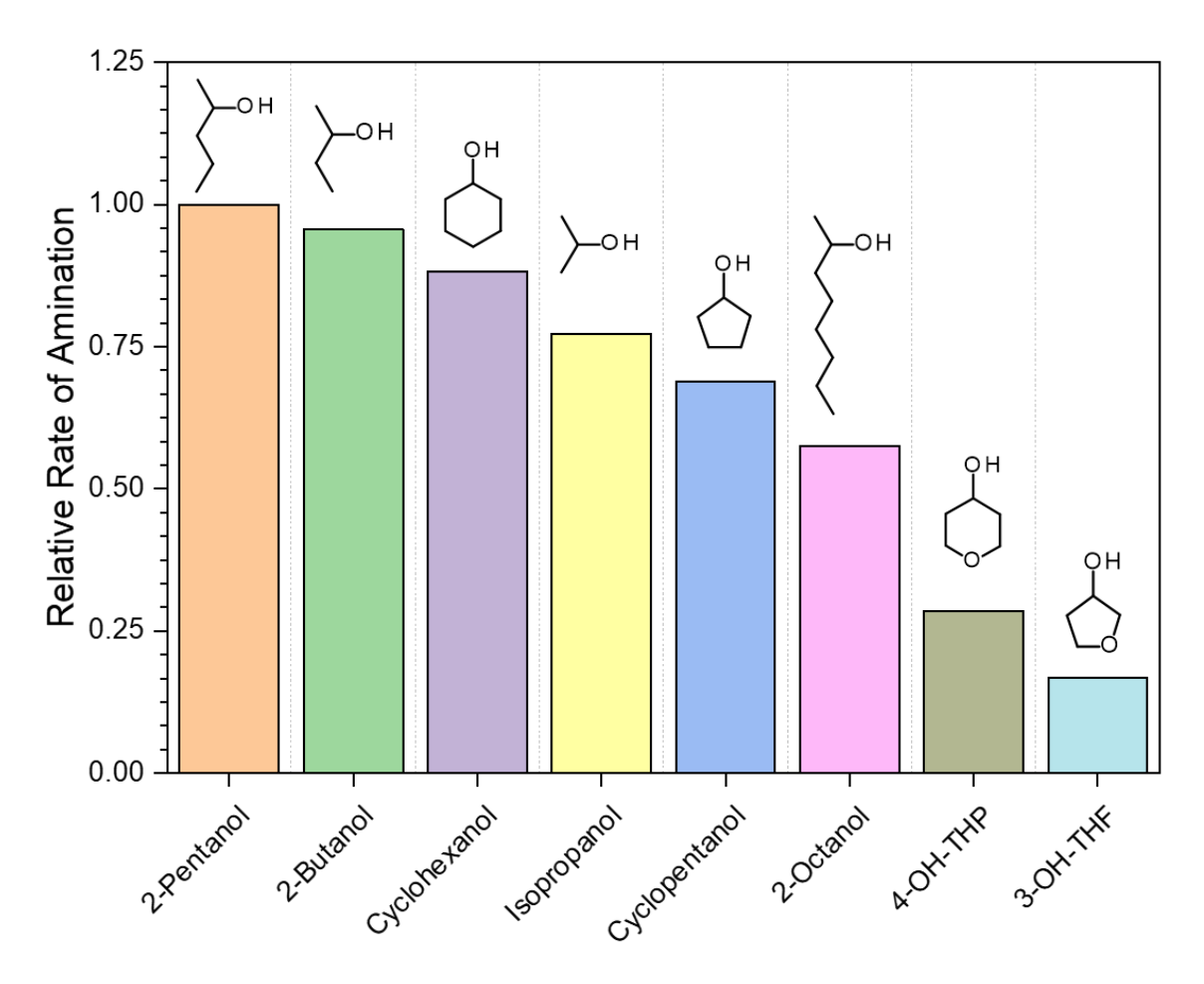


Figure 12: Rates of amination for various aliphatic and heterocyclic secondary alcohols over Ru/SiO₂-A (0.6 wt% Ru) at T = 433K, pOH = 1.3×10^{-3} bar, pH₂ = 0.20 bar, pNH₃ = 0.20 bar, He balance. All rates of reaction are normalized to the rate of amination observed for 2-pentanol.

We next considered amination of each of the above substrates over a range of conditions, adjusting partial pressures and residence times as needed to permit efficient vaporization of the substrate and facilitate high conversion. Results are summarized in Table 5. Considering Entries 1-6, we conclude that amination of monofunctional secondary alcohols is relatively straightforward, and that primary amine yields between 70-90% are attainable at residence times below 1 ks for modest pressures of H_2 (0.60 bar) and NH_3 (0.40 bar). It is also possible to obtain primary amine yields in excess of 90% during amination of the heterocyclic alcohol 4-OH-THP (Entry 7); however, it requires a significant increase in H_2 pressure (1.12 bar), NH_3 pressure (3.34 bar), and residence time (2.8 ks). The only exception was 3-OH-THF, for which we observed a maximum

yield of only 51% despite forcing conditions and a long residence time (Entry 8). This decrease in amination activity for heterocyclic alcohols is consistent with diminished conversions and amine yields previously reported during the amination of 1-octanol, 2-butanol, and furfuryl alcohol over Ru nanoparticles at 453K.⁷

Table 5: Primary amine yields under optimal conditions for various secondary alcohols

Entry	Secondary alcohol	Alcohol (bar)	NH ₃ (bar)	H ₂ (bar)	τ (ks)	Yield
1	Isopropanol	0.021	0.40	0.60	0.17	0.73
2	2-Butanol	0.021	0.40	0.60	0.18	0.76
3	2-Pentanol	0.021	0.40	0.60	0.18	0.76
4	Cyclopentanol	0.011	0.40	0.60	0.35	0.80
5	Cyclohexanol	0.005	0.40	0.60	0.70	0.93
6	2-Octanol	0.003	0.40	0.61	0.70	0.79
7	4-OH-THP	0.003	3.34	1.12	2.84	0.90
8	3-OH-THF	0.003	3.34	1.12	2.86	0.51

T = 433K, Ru/SiO₂-C (3.3 wt%)

To gain further insight, we examined trends in fractional conversion and amination site time yield as a function of residence time during the amination of 3-OH-THF at T=433K, $p_{OH}=1.3\times 10^{-3}$ bar, $p_{NH3}=0.41$ bar, and $p_{H2}=0.61$ bar (Figure 13). As residence times increase from 0 to 3ks, we observe a substantial decline in amination rate, and we observe a plateau in fractional conversion at ≈ 0.3 . We can propose three explanations for this behavior. The first is

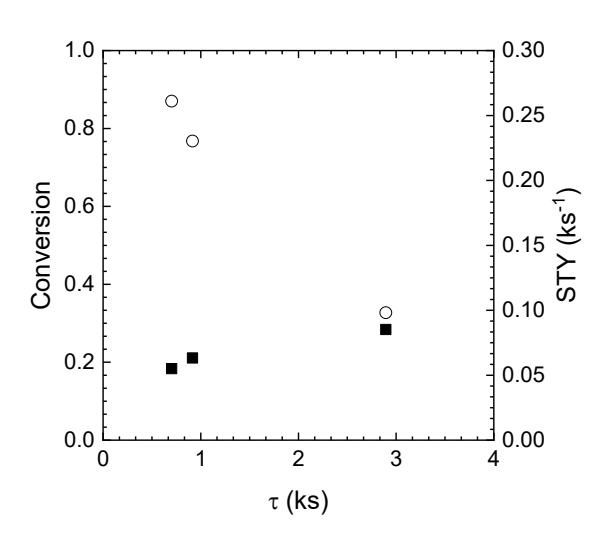


Figure 13. Conversion (■) and amination site time yields (○) observed as a function of contact time during the reductive amination of 3OH-THF over Ru/SiO₂-C (3.3 wt% Ru) at T = 433K, $p_{OH} = 1.33 \times 10^{-3}$ bar, $p_{H2} = 0.61$ bar, $p_{NH3} = 0.41$ bar.

that, unlike amination of monofunctional alcohols, the amination of heterocycles has an unfavorable equilibrium position and so attains a maximum conversion of only 30% under the reported conditions. The second is that the catalyst experiences product inhibition such that its

activity decreases as a function of reaction progress. The final is that the catalyst is deactivating over the course of the experiment. We exclude the latter because these experiments were performed in a packed bed operating at steady state, and data points in Figure 13 reflect average conversions and site time yields obtained over 5 hours of continuous operation. During these experiments, we observed no loss of activity as a function of time on stream. This leaves only thermodynamic limitations and product inhibition as underlying causes of the conversion plateau; accordingly, we next consider the free energy of heterocycle amination.

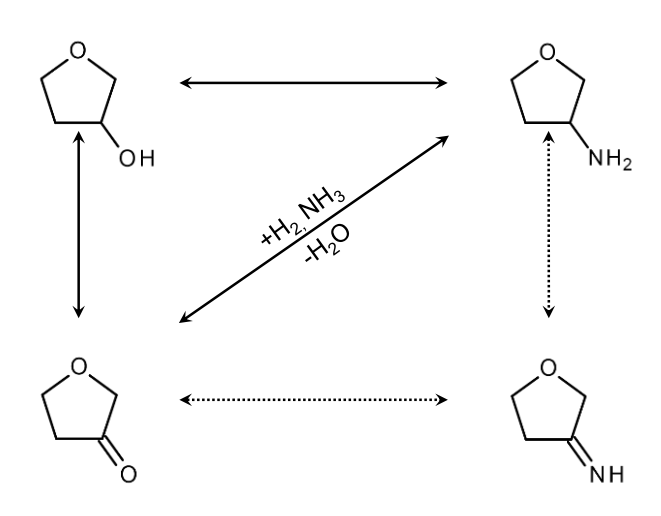


Figure 14: Macroscopic reactions occurring during the amination of 3-OH-THF to form 3-NH₂-THF. Pathway (1) represents the formation of 3-NH₂-THF through direct amination. Pathways (2) and (3) comprise the formation of a 3-NH₂-THF by secondary amination of 3-OXO-THF that is initially formed by dehydrogenation of 3-OH-THF. Dashed lines describe the formation and consumption of the presumed imine intermediate, 3-NH-THF.

To aid visualization, Figure 14 maps generic reactions that are anticipated to occur during alcohol animation (Figure 1) onto the amination of 3-OH-THF. According to computational data, the overall amination of 3-OH-THF (Reaction 1) is thermoneutral ($\Delta H \approx -0.030 \text{ kJ mol}^{-1}$, $\Delta S \approx -2 \text{ J mol}^{-1} \text{ K}^{-1}$). As such, if one considers only the amination of 3-OH-THF without intermediate formation of 3-OXO-THF, the equilibrium yield to 3-NH₂-THF

under the reported conditions exceeds 99%. That said, the dehydrogenation of 3-OH-THF to form 3-OXO-THF (Reaction 2) is favorable ($\Delta H \approx$ -30 kJ mol-1, $\Delta S \approx$ 120 J mol⁻¹ K⁻¹), whereas the subsequent reductive amination of 3-OXO-THF to form 3-NH₂-THF (Reaction 3) is unfavorable ($\Delta H \approx$ 30 kJ mol⁻¹, $\Delta S \approx$ -120 J mol⁻¹ K⁻¹). This means that, under conditions where the dehydrogenation of 3-OH-THF and the amination of 3-OXO-THF are both kinetically accessible,

one expects to observe near-complete conversion of 3-OH-THF and near-quantitative selectivity to 3-OXO-THF. Thermodynamic constraints may therefore limit attainable yields to 3-NH₂-THF, but they should not restrict the conversion of 3-OH-THF to \approx 30% under amination conditions.

Table 6: Binding Energies for Various Secondary Alcohols

Entry	Secondary alcohol	BE (eV)
1	2-Butanol	0.97
2	Cyclopentanol	1.19
3	3-OH-THF	1.44

More likely, the decrease in reaction rate and fractional conversion illustrated in Figure 13 are associated with inhibition by strongly bound reaction intermediates/products or spectator species that accumulate at higher feed conversion. This interpretation is consistent with calculated binding energies (Table 6), which show that 3-OH-THF binds strongly on Ru (1.44 eV) relative to a linear C₄ alcohol (2-butanol, 0.97 eV) and a cyclic C₅ alcohol (cyclopentanol, 1.19 eV). 3-OH-THF binds more strongly because its two oxygen atoms facilitate bidentate coordination to the Ru surface (Figure 15). This configuration is significantly more stable than analogous monodentate adsorption modes for secondary alcohols. Presumably, this trend extends to heterocyclic intermediates (e.g., 3-OXO-THF, 3-NH-THF) and reaction products (3-NH₂-THF), which supports the argument that product inhibition through stable binding of heterocyclic species underlies the loss of activity with increasing residence time.

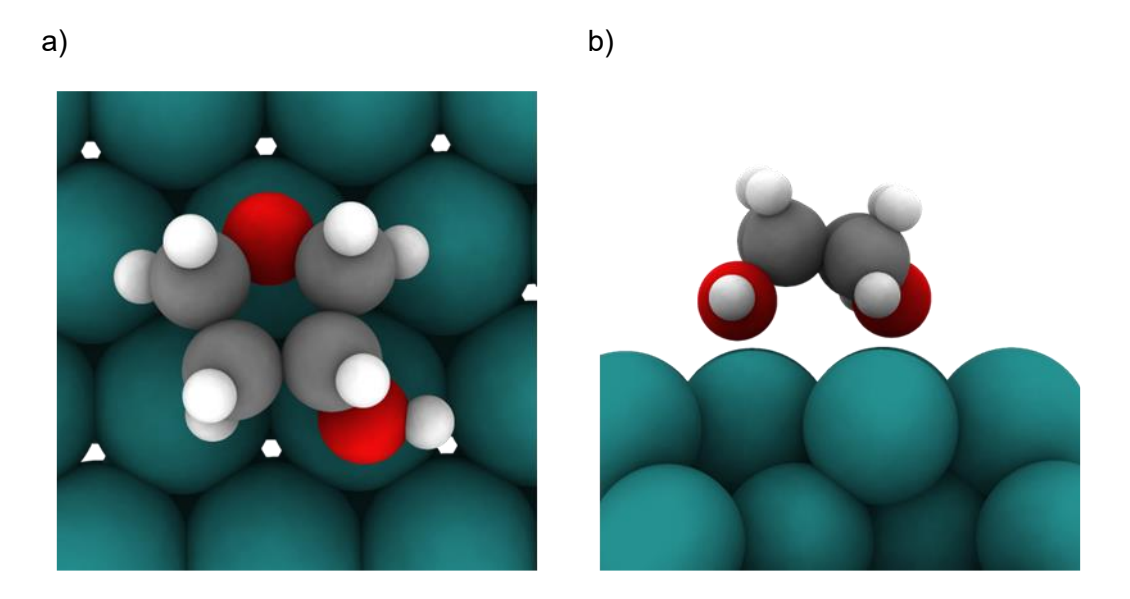


Figure 15: Top (a) and side (b) views of the favorable adsorption geometry of 3-OH-THF over Ru(0001).

Finally, from a practical standpoint, vapor-phase amination is viable mainly for short chain alcohols. Substrates with higher molecular weight and/or lower vapor pressures will benefit from condensed-phase processing. To determine whether gas-phase insights are generally extensible, we consider the reductive amination of 2-octanol dissolved in n-decane at a mole fraction of 6.7 × 10⁻³. We find that insights from gas-phase amination translate directly to liquid-phase amination, and we achieve 2-octanamine yields in excess of 90% by operating at 423 or 433K under 6.4 bar NH₃ and 13.6 bar H₂ (Figure 16). Although good primary amine selectivity is also observed at 413K, it requires long reaction times and/or catalyst loadings to achieve high conversion. In contrast, by operating at 443K, we see a significant increase in the rate of conversion, but this is accompanied by a loss in amine selectivity and incomplete carbon balance closure (+/- 30%). This is presumably attributed to the formation of gas-phase hydrocarbons, which were not measured for liquid-phase reactions.

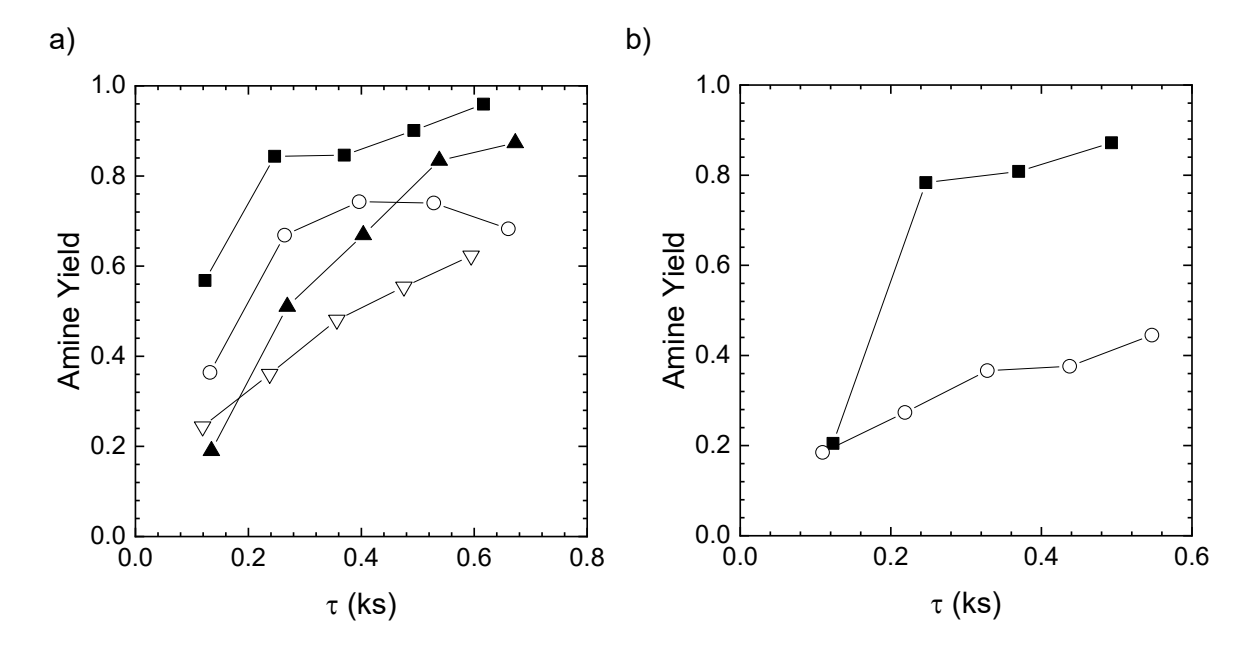


Figure 16. a) Amine yields observed as a function of contact time during the reductive amination of 2-octanol in decane over Ru/SiO₂-D (14.6 wt% Ru) at $x_{OH} = 6.7 \times 10^{-3}$, $p_{H2} = 13.6$ bar, $p_{NH3} = 6.4$ bar and 398K (∇), 413K (\triangle), 433K (\blacksquare), and 443K (\circ). b) Amine yields observed as a function of contact time during the reductive amination of 2-octanol in decane at 423K under 13.6 bar H₂ (\blacksquare) and under 0 bar H₂ (\circ) over Ru/SiO₂-D (14.6 wt% Ru) and at $x_{OH} = 6.7 \times 10^{-3}$, $p_{NH3} = 6.5$ bar, and He = balance.

As demonstrated by Shimizu, external hydrogen is not required for the amination of secondary alcohols. ¹³¹ Reducing environments clearly benefit catalyst stability (Figure 7), but operating in excess H_2 adds additional cost and expands the carbon footprint of alcohol amination. It is thus noteworthy that one can obtain 45% yields of 2-octanamine under 6.4 bar NH₃ after ≈ 0.6 ks (0.17h) using a 14.6 wt.% Ru/SiO₂ catalyst, even if H_2 is replaced entirely by He (Figure 16b). This is comparable to 2-octanamine yields obtained during the hydrogen-free amination of 2-octanol under 4 bar of NH₃ over 5 wt.% Ru/ γ -Al₂O₃ by Shimizu (4h), but lower than the 2-octanimine yields that they reported over a 10 wt.% Ni/Al₂O₃ catalyst under the same conditions (>80%). ¹³² From the yield curves in Figure 16b, it is clear that amination rates are lower in the absence of H_2 . Based on insights from gas-phase experiments, we tentatively attribute this to deactivation of the catalyst rather than a positive hydrogen order—this is supported by the fact that both systems

achieve similar amine yields at short residence times (0.12 ks), whereafter the two systems diverge. Despite this, there are potential benefits to operating without H₂. For example, operating under N₂ or He (instead of H₂) would minimize hydrogenolysis and/or hydrogenation reactions that lead to alkane formation. Considering that the main loss of selectivity is to hydrocarbon formation, further optimization of H₂-free alcohol amination systems may be warranted, and prior work by Shimizu suggests that higher yields are possible with an extension of residence times under inert atmospheres.¹³²

Conclusions

Thermodynamically, amination of secondary alcohols with ammonia to form primary amines is favorable under typical reaction conditions (400 – 500K); however, it occurs in parallel (and in series) with alcohol dehydrogenation. As such, one should anticipate that reaction products will be a mixture of carbonyls and primary amines. At low temperatures (<500K), equilibrium favors amine production, whereas carbonyls become thermodynamically favored at high temperatures (>600K). For the substrates considered here, we find that near quantitative yields of primary amines are thermodynamically accessible from 400 – 450K when operating under excess NH₃.

In terms of reactor operation, there are multiple tradeoffs to consider in maximizing conversion rate, selectivity, and yield to primary amines. Species partial pressure, reaction temperature, residence time, and the molecular structure of the alcohol substrate all influence reactivity and selectivity. Strictly speaking, dihydrogen is not necessary for alcohol amination. Further, variations in H₂ pressure have minimal impact on the *intrinsic* rate of amination and product selectivity. However, elevated H₂ pressures improve catalyst stability, so a hydrogen co-feed remains beneficial. A potential consideration is that alcohol amination proceeds at least partially through a dehydrogenation step to form a carbonyl compound, and dehydrogenation is

thermodynamically unfavorable below 500K, especially at elevated H₂ pressures. That said, we observe no significant impediments to alcohol amination under these conditions, and we find that good primary amine yields are attainable between 400 – 450K under excess H₂. Next, increasing ammonia pressure significantly improves amine selectivity while inhibiting isopropanol conversion. Specifically, increasing ammonia pressure suppresses the rate of alcohol dehydrogenation without affecting the apparent rate of alcohol amination. For this reason, if targeting the synthesis of primary amines, there is no obvious kinetic drawback to operating at high ammonia pressures to promote amine selectivity. In contrast, increasing alcohol pressure enhances the rate of alcohol conversion, but it favors dehydrogenation instead of amination, so operating under alcohol-rich conditions is detrimental to amine selectivity. That said, this is not a catastrophic loss since the carbonyl formed by alcohol dehydrogenation is a reaction intermediate that can ultimately be converted to a primary amine via reductive amination. Concentrated isopropanol feeds are desirable in practice as they facilitate process intensification, but this may come at the cost of catalyst stability, which is best under excess NH₃ and H₂. Although insights were generated during the amination of isopropanol in a differential packed bed, they are extensible to other substrates, and we find that Ru/SiO₂ is an effective catalyst for the amination of secondary alcohols in vapor and liquid media and using batch and flow reactors. Moreover, similarities between trends reported here and in prior analyses of n-alcohol amination suggest that conclusions presented here may also generalize to the amination of primary alcohols. Operating between 400 and 450K, we generally observe complete conversion of alcohols within practical residence times (< 20 minutes). It is also possible to maintain good selectivity toward primary amines, and yields of 70 - 90% are feasible for most secondary alcohols. An important caveat is that heterocyclic alcohols based on pyran and furan ring structures appear susceptible to product

inhibition, which presumably arises because these species can bind in favorable, bidentate configurations that leads to poisoning of the catalyst surface. Despite this, it is generally possible to improve yields during the amination of 4-hydroxytetrahydropyran and 3-hydroxytetrahydrofuran by increasing ammonia and H₂ pressures. Finally, under the conditions reported herein over Ru/SiO₂, one avoids sequential amination reactions that lead to secondary and tertiary amines, which is a longstanding selectivity challenge in the amination of ketones and alkyl halides.

Conflicts of interest

The authors declare no conflicts of interest.

Acknowledgements

J.Q.B. and X.G. acknowledge financial support from the National Science Foundation under Grant No. CBET-1804843. D.S. and A.H. acknowledge financial support from the National Science Foundation under Grant No. CBET-1805307 and the South Carolina State Center for Strategic Approaches to the Generation of Electricity (SAGE). Computing resources have been provided by the National Energy Research Scientific Computing Center (NERSC) under Contract No. DE-AC02-05CH11231 and Pacific Northwest National Laboratory (Ringgold ID 130367, Grant Proposal 51711), XSEDE facilities located at San Diego Supercomputer Center (SDSC) and Texas advanced Computing Center (TACC) under grant number TG-CTS090100, and the High-Performance Computing clusters located at University of South Carolina.

References

N. Mizuno, M. Tabata, T. Uematsu and M. Iwamoto, in *Studies in Surface Science and Catalysis*, eds. H. Hattori, M. Misono and Y. Ono, Elsevier, 1994, vol. 90, pp. 71–76.

- 2 M. Lequitte, F. Figueras, C. Moreau and S. Hub, Amination of Butenes over Protonic Zeolites, *J. Catal.*, 1996, **163**, 255–261.
- T. E. Müller and M. Beller, Metal-Initiated Amination of Alkenes and Alkynes, *Chem. Rev.*, 1998, **98**, 675–704.
- J. Penzien, R. Q. Su and T. E. Müller, The role of protons in hydroamination reactions involving homogeneous and heterogeneous catalysts, *J. Mol. Catal. Chem.*, 2002, **182–183**, 489–498.
- 5 C. R. Ho, L. A. Bettinson, J. Choi, M. Head-Gordon and A. T. Bell, Zeolite-Catalyzed Isobutene Amination: Mechanism and Kinetics, *ACS Catal.*, 2019, **9**, 7012–7022.
- 6 E. Podyacheva, O. I. Afanasyev, D. V. Vasilyev and D. Chusov, Borrowing Hydrogen Amination Reactions: A Complex Analysis of Trends and Correlations of the Various Reaction Parameters, *ACS Catal.*, 2022, **12**, 7142–7198.
- 7 G. Liang, Y. Zhou, J. Zhao, A. Y. Khodakov and V. V. Ordomsky, Structure-Sensitive and Insensitive Reactions in Alcohol Amination over Nonsupported Ru Nanoparticles, ACS Catal., 2018, 8, 11226–11234.
- 8 X.-P. Fu, P. Han, Y.-Z. Wang, S. Wang and N. Yan, Insight into the roles of ammonia during direct alcohol amination over supported Ru catalysts, *J. Catal.*, 2021, **399**, 121–131.
- Yu. S. Demidova, E. V. Suslov, I. L. Simakova, E. S. Mozhajcev, D. V. Korchagina, K. P. Volcho, N. F. Salakhutdinov, A. Simakov and D. Yu. Murzin, One-pot monoterpene alcohol amination over Au/ZrO2 catalyst: Effect of the substrate structure, *J. Catal.*, 2018, 360, 127–134.
- 10 S. Bähn, S. Imm, L. Neubert, M. Zhang, H. Neumann and M. Beller, The Catalytic Amination of Alcohols, *ChemCatChem*, 2011, **3**, 1853–1864.
- 11 S. Gomez, J. A. Peters and T. Maschmeyer, The Reductive Amination of Aldehydes and Ketones and the Hydrogenation of Nitriles: Mechanistic Aspects and Selectivity Control, *Adv. Synth. Catal.*, 2002, **344**, 1037–1057.
- 12 A. Cukalovic and C. V. Stevens, Production of biobased HMF derivatives by reductive amination, *Green Chem.*, 2010, **12**, 1201–1206.
- 13 T. Irrgang and R. Kempe, Transition-Metal-Catalyzed Reductive Amination Employing Hydrogen, *Chem. Rev.*, 2020, **120**, 9583–9674.
- 14 Y. Nakamura, K. Kon, A. S. Touchy, K. Shimizu and W. Ueda, Selective Synthesis of Primary Amines by Reductive Amination of Ketones with Ammonia over Supported Pt catalysts, *ChemCatChem*, 2015, 7, 921–924.
- 15 G. F. Liang, A. Q. Wang, L. Li, G. Xu, N. Yan and T. Zhang, Production of Primary Amines by Reductive Amination of Biomass-Derived Aldehydes/Ketones, *Angew. Chem.-Int. Ed.*, 2017, **56**, 3050–3054.
- 16 J. M. Carraher, C. N. Fleitman and J.-P. Tessonnier, Kinetic and Mechanistic Study of Glucose Isomerization Using Homogeneous Organic Brønsted Base Catalysts in Water, ACS Catal., 2015, 5, 3162–3173.
- 17 C. Liu, J. M. Carraher, J. L. Swedberg, C. R. Herndon, C. N. Fleitman and J.-P. Tessonnier, Selective Base-Catalyzed Isomerization of Glucose to Fructose, *ACS Catal.*, 2014, **4**, 4295–4298.
- 18 E. S. Sanz-Pérez, C. R. Murdock, S. A. Didas and C. W. Jones, Direct Capture of CO₂ from Ambient Air, *Chem. Rev.*, 2016, **116**, 11840–11876.
- 19 Y. Li, Y. Tang, S. Zhang and J. Yang, Synthesis and Application of Crosslinking Blue Anthraquinone Polyamine Dye with High Fixation, *Text. Res. J.*, 2007, **77**, 703–709.

- 20 Y. Li, S. Zhang, J. Yang, S. Jiang and Q. Li, Synthesis and application of novel crosslinking polyamine dyes with good dyeing performance, *Dyes Pigments*, 2008, **76**, 508–514.
- 21 O. Saidi, A. J. Blacker, M. M. Farah, S. P. Marsden and J. M. J. Williams, Selective Amine Cross-Coupling Using Iridium-Catalyzed "Borrowing Hydrogen" Methodology, *Angew. Chem.*, 2009, **121**, 7511–7514.
- 22 O. I. Afanasyev, E. Kuchuk, D. L. Usanov and D. Chusov, Reductive Amination in the Synthesis of Pharmaceuticals, *Chem. Rev.*, 2019, **119**, 11857–11911.
- 23 P. Tufvesson, J. Lima-Ramos, J. S. Jensen, N. Al-Haque, W. Neto and J. M. Woodley, Process considerations for the asymmetric synthesis of chiral amines using transaminases, *Biotechnol. Bioeng.*, 2011, **108**, 1479–1493.
- 24 V. Gotor-Fernández, R. Brieva and V. Gotor, Lipases: Useful biocatalysts for the preparation of pharmaceuticals, *J. Mol. Catal. B Enzym.*, 2006, **40**, 111–120.
- 25 T. Cernak, K. D. Dykstra, S. Tyagarajan, P. Vachal and S. W. Krska, The medicinal chemist's toolbox for late stage functionalization of drug-like molecules, *Chem. Soc. Rev.*, 2016, **45**, 546–576.
- 26 R. V. Jagadeesh, K. Murugesan, A. S. Alshammari, H. Neumann, M.-M. Pohl, J. Radnik and M. Beller, MOF-derived cobalt nanoparticles catalyze a general synthesis of amines, *Science*, 2017, 358, 326–332.
- 27 K. Murugesan, T. Senthamarai, V. G. Chandrashekhar, K. Natte, P. C. J. Kamer, M. Beller and R. V. Jagadeesh, Catalytic reductive aminations using molecular hydrogen for synthesis of different kinds of amines, *Chem. Soc. Rev.*, 2020, **49**, 6273–6328.
- 28 E. Nauha and M. Nissinen, Co-crystals of an agrochemical active A pyridine-amine synthon for a thioamide group, *J. Mol. Struct.*, 2011, **1006**, 566–569.
- 29 B. Manteau, S. Pazenok, J.-P. Vors and F. R. Leroux, New trends in the chemistry of α-fluorinated ethers, thioethers, amines and phosphines, *J. Fluor. Chem.*, 2010, **131**, 140–158.
- 30 M. Höhne and U. T. Bornscheuer, Biocatalytic Routes to Optically Active Amines, *ChemCatChem*, 2009, **1**, 42–51.
- 31 A. Corma, J. Navas and M. J. Sabater, Advances in One-Pot Synthesis through Borrowing Hydrogen Catalysis, *Chem. Rev.*, 2018, **118**, 1410–1459.
- 32 Q. Yang, Q. Wang and Z. Yu, Substitution of alcohols by N-nucleophiles via transition metal-catalyzed dehydrogenation, *Chem. Soc. Rev.*, 2015, **44**, 2305–2329.
- 33 R. N. Salvatore, C. H. Yoon and K. W. Jung, Synthesis of secondary amines, *Tetrahedron*, 2001, **57**, 7785–7811.
- 34 C. Li, X. Zhao, A. Wang, G. W. Huber and T. Zhang, Catalytic Transformation of Lignin for the Production of Chemicals and Fuels, *Chem. Rev.*, 2015, **115**, 11559–11624.
- 35 D. Martin Alonso, J. Q. Bond and J. A. Dumesic, Catalytic Conversion of Biomass to Biofuels, *Green Chem.*, 2010, **12**, 1493–1513.
- 36 L. R. Lynd, J. H. Cushman, R. J. Nichols and C. E. Wyman, Fuel Ethanol from Cellulosic Biomass, *Science*, 1991, **251**, 1318–1323.
- 37 S. Imm, S. Bähn, L. Neubert, H. Neumann and M. Beller, An Efficient and General Synthesis of Primary Amines by Ruthenium-Catalyzed Amination of Secondary Alcohols with Ammonia, *Angew. Chem. Int. Ed.*, 2010, **49**, 8126–8129.
- 38 M. Pera-Titus and F. Shi, Catalytic Amination of Biomass-Based Alcohols, *ChemSusChem*, 2014, 7, 720–722.

- 39 B. Dong, X. Guo, B. Zhang, X. Chen, J. Guan, Y. Qi, S. Han and X. Mu, Heterogeneous Ru-Based Catalysts for One-Pot Synthesis of Primary Amines from Aldehydes and Ammonia, *Catalysts*, 2015, **5**, 2258–2270.
- 40 G. Guillena, D. J. Ramón and M. Yus, Hydrogen Autotransfer in the N-Alkylation of Amines and Related Compounds using Alcohols and Amines as Electrophiles, *Chem. Rev.*, 2010, **110**, 1611–1641.
- 41 T. Wang, J. Ibañez, K. Wang, L. Fang, M. Sabbe, C. Michel, S. Paul, M. Pera-Titus and P. Sautet, Rational design of selective metal catalysts for alcohol amination with ammonia, *Nat. Catal.*, 2019, **2**, 773–779.
- 42 C. R. Ho, V. Defalque, S. Zheng and A. T. Bell, Propanol Amination over Supported Nickel Catalysts: Reaction Mechanism and Role of the Support, *ACS Catal.*, 2019, **9**, 2931–2939.
- 43 S. Li, M. Wen, H. Chen, Z. Ni, J. Xu and J. Shen, Amination of isopropanol to isopropylamine over a highly basic and active Ni/LaAlSiO catalyst, *J. Catal.*, 2017, **350**, 141–148.
- 44 V. A. Veefkind and J. A. Lercher, On the elementary steps of acid zeolite catalyzed amination of light alcohols, *Appl. Catal. Gen.*, 1999, **181**, 245–255.
- 45 J. Soto, J. M. Rosas, J. C. Otero, J. Rodríguez-Mirasol and T. Cordero, Reaction Mechanisms of 2-Butanol Dehydration over a Phosphorus-Containing Activated Carbon Acid Catalyst, *J. Phys. Chem. C*, 2018, **122**, 16772–16778.
- 46 T. K. Phung and G. Busca, Diethyl ether cracking and ethanol dehydration: Acid catalysis and reaction paths, *Chem. Eng. J.*, 2015, **272**, 92–101.
- 47 C. P. Nash, A. Ramanathan, D. A. Ruddy, M. Behl, E. Gjersing, M. Griffin, H. Zhu, B. Subramaniam, J. A. Schaidle and J. E. Hensley, Mixed alcohol dehydration over Brønsted and Lewis acidic catalysts, *Appl. Catal. Gen.*, 2016, **510**, 110–124.
- 48 W. E. Farneth and R. J. Gorte, Methods for Characterizing Zeolite Acidity, *Chem. Rev.*, 1995, **95**, 615–635.
- 49 J. G. Tittensor, R. J. Gorte and D. M. Chapman, Isopropylamine adsorption for the characterization of acid sites in silica-alumina catalysts, *J. Catal.*, 1992, **138**, 714–720.
- 50 M. H. S. A. Hamid, C. L. Allen, G. W. Lamb, A. C. Maxwell, H. C. Maytum, A. J. A. Watson and J. M. J. Williams, Ruthenium-Catalyzed N-Alkylation of Amines and Sulfonamides Using Borrowing Hydrogen Methodology, *J. Am. Chem. Soc.*, 2009, **131**, 1766–1774.
- 51 C. Gunanathan and D. Milstein, Applications of Acceptorless Dehydrogenation and Related Transformations in Chemical Synthesis, *Science*, 2013, **341**, 1229712.
- 52 A. Baiker, W. Caprez and W. L. Holstein, Catalytic amination of aliphatic alcohols in the gas and liquid phases: kinetics and reaction pathway, *Ind. Eng. Chem. Prod. Res. Dev.*, 1983, **22**, 217–225.
- 53 T. Senthamarai, K. Murugesan, J. Schneidewind, N. V. Kalevaru, W. Baumann, H. Neumann, P. C. J. Kamer, M. Beller and R. V. Jagadeesh, Simple ruthenium-catalyzed reductive amination enables the synthesis of a broad range of primary amines, *Nat. Commun.*, 2018, **9**, 4123.
- 54 K. Murugesan, Z. Wei, V. G. Chandrashekhar, H. Neumann, A. Spannenberg, H. Jiao, M. Beller and R. V. Jagadeesh, Homogeneous cobalt-catalyzed reductive amination for synthesis of functionalized primary amines, *Nat. Commun.*, 2019, **10**, 5443.

- 55 B. G. Reed-Berendt, K. Polidano and L. C. Morrill, Recent advances in homogeneous borrowing hydrogen catalysis using earth-abundant first row transition metals, *Org. Biomol. Chem.*, 2019, **17**, 1595–1607.
- 56 M. R. Ball, T. S. Wesley, K. R. Rivera-Dones, G. W. Huber and J. A. Dumesic, Amination of 1-hexanol on bimetallic AuPd/TiO ₂ catalysts, *Green Chem.*, 2018, **20**, 4695–4709.
- 57 N. S. Gould, H. Landfield, B. Dinkelacker, C. Brady, X. Yang and B. Xu, Selectivity Control in Catalytic Reductive Amination of Furfural to Furfurylamine on Supported Catalysts, *ChemCatChem*, 2020, **12**, 2106–2115.
- 58 F. Niu, M. Bahri, O. Ersen, Z. Yan, B. T. Kusema, A. Y. Khodakov and V. V. Ordomsky, A multifaceted role of a mobile bismuth promoter in alcohol amination over cobalt catalysts, *Green Chem.*, 2020, **22**, 4270–4278.
- 59 S. Song, Y. Wang and N. Yan, A remarkable solvent effect on reductive amination of ketones, *Mol. Catal.*, 2018, **454**, 87–93.
- 60 A. Baiker and W. Richarz, Catalytic Amination of Long Chain Aliphatic Alcohols, *Prod. RD*, 1977, **16**, 261–266.
- 61 G. Sewell, C. O'Connor and E. van Steen, Reductive amination of ethanol with silica-supported cobalt and nickel catalysts, *Appl. Catal. Gen.*, 1995, **125**, 99–112.
- 62 A. S. Dumon, T. Wang, J. Ibañez, A. Tomer, Z. Yan, R. Wischert, P. Sautet, M. Pera-Titus and C. Michel, Direct n-octanol amination by ammonia on supported Ni and Pd catalysts: activity is enhanced by "spectator" ammonia adsorbates, *Catal. Sci. Technol.*, 2018, **8**, 611–621.
- 63 Y. Kita, M. Kuwabara, S. Yamadera, K. Kamata and M. Hara, Effects of ruthenium hydride species on primary amine synthesis by direct amination of alcohols over a heterogeneous Ru catalyst, *Chem. Sci.*, 2020, **11**, 9884–9890.
- 64 D. Ruiz, A. Aho, P. Mäki-Arvela, N. Kumar, H. Oliva and D. Yu. Murzin, Direct Amination of Dodecanol over Noble and Transition Metal Supported Silica Catalysts, *Ind. Eng. Chem. Res.*, 2017, **56**, 12878–12887.
- 65 O. A. Abdelrahman, A. Heyden and J. Q. Bond, Microkinetic analysis of C3–C5 ketone hydrogenation over supported Ru catalysts, *J. Catal.*, 2017, **348**, 59–74.
- 66 O. A. Abdelrahman, A. Heyden and J. Q. Bond, Analysis of kinetics and reaction pathways in the aqueous-phase hydrogenation of levulinic acid to form γ-valerolactone over Ru/C, *ACS Catal.*, 2014, **4**, 1171–1181.
- 67 O. A. Abdelrahman, H. Y. Luo, A. Heyden, Y. Román-Leshkov and J. Q. Bond, Toward rational design of stable, supported metal catalysts for aqueous-phase processing: Insights from the hydrogenation of levulinic acid, *J. Catal.*, 2015, **329**, 10–21.
- 68 D. Martin Alonso, J. Q. Bond, J. C. Serrano-Ruiz and J. A. Dumesic, Production of liquid hydrocarbon transportation fuels by oligomerization of biomass-derived C9 alkenes, *Green Chem.*, 2010, **12**, 992–999.
- 69 D. Martin Alonso, J. Q. Bond, D. Wang and J. A. Dumesic, Activation of Amberlyst-70 for Alkene Oligomerization in Hydrophobic media, *Top. Catal*.
- 70 C. Michel, J. Zaffran, A. M. Ruppert, J. Matras-Michalska, M. Jedrzejczyk, J. Grams and P. Sautet, Role of water in metal catalyst performance for ketone hydrogenation: a joint experimental and theoretical study on levulinic acid conversion into gamma-valerolactone, *Chem. Commun.*, 2014, **50**, 12450–12453.

- 71 C. Delhomme, L. A. Schaper, M. Zhang-Presse, G. Raudaschl-Sieber, D. Weuster-Botz and F. E. Kuhn, Catalytic hydrogenation of levulinic acid in aqueous phase, *J. Organomet. Chem.*, 2013, **724**, 297–299.
- 72 L. E. Manzer, Catalytic synthesis of alpha-methylene-gamma-valerolactone: a biomass-derived acrylic monomer, *Appl. Catal. Gen.*, 2004, **272**, 249–256.
- 73 W. H. Luo, M. Sankar, A. M. Beale, Q. He, C. J. Kiely, P. C. A. Bruijnincx and B. M. Weckhuysen, High performing and stable supported nano-alloys for the catalytic hydrogenation of levulinic acid to gamma-valerolactone, *Nat. Commun.*, , DOI:10.1038/ncomms7540.
- 74 A. S. Piskun, J. Ftouni, Z. Tang, B. M. Weckhuysen, P. C. A. Bruijnincx and H. J. Heeres, Hydrogenation of levulinic acid to gamma-valerolactone over anatase-supported Ru catalysts: Effect of catalyst synthesis protocols on activity, *Appl. Catal. -Gen.*, 2018, **549**, 197–206.
- 75 O. Mamun, M. Saleheen, J. Q. Bond and A. Heyden, Investigation of solvent effects in the hydrodeoxygenation of levulinic acid to γ-valerolactone over Ru catalysts, *J. Catal.*, 2019, 379, 164–179.
- 76 S. Cao, J. R. Monnier, C. T. Williams, W. J. Diao and J. R. Regalbuto, Rational nanoparticle synthesis to determine the effects of size, support, and K dopant on Ru activity for levulinic acid hydrogenation to gamma-valerolactone, *J. Catal.*, 2015, **326**, 69–81.
- 77 H. Junge, B. Loges and M. Beller, Novel improved ruthenium catalysts for the generation of hydrogen from alcohols, *Chem. Commun.*, 2007, 522–524.
- 78 J. Gallardo-Donaire, M. Ernst, O. Trapp and T. Schaub, Direct Synthesis of Primary Amines via Ruthenium-Catalysed Amination of Ketones with Ammonia and Hydrogen, *Adv. Synth. Catal.*, 2016, **358**, 358–363.
- 79 D. Pingen, C. Müller and D. Vogt, Direct Amination of Secondary Alcohols Using Ammonia, *Angew. Chem. Int. Ed.*, 2010, **49**, 8130–8133.
- 80 A. B. Enyong and B. Moasser, Ruthenium-Catalyzed N-Alkylation of Amines with Alcohols under Mild Conditions Using the Borrowing Hydrogen Methodology, *J. Org. Chem.*, 2014, 79, 7553–7563.
- 81 X. Ye, P. N. Plessow, M. K. Brinks, M. Schelwies, T. Schaub, F. Rominger, R. Paciello, M. Limbach and P. Hofmann, Alcohol Amination with Ammonia Catalyzed by an Acridine-Based Ruthenium Pincer Complex: A Mechanistic Study, *J. Am. Chem. Soc.*, 2014, **136**, 5923–5929.
- 82 J. Bódis, L. Lefferts, T. E. Müller, R. Pestman and J. A. Lercher, Activity and Selectivity Control in Reductive Amination of Butyraldehyde over Noble Metal Catalysts, *Catal. Lett.*, 2005, **104**, 23–28.
- 83 T. P. Vispute, H. Zhang, A. Sanna, R. Xiao and G. W. Huber, Renewable Chemical Commodity Feedstocks from Integrated Catalytic Processing of Pyrolysis Oils, *Science*, 2010, **330**, 1222–1227.
- 84 V. K. Tandon, A. M. Van Leusen and H. Wynberg, Synthesis of enantiomerically pure (S)-(+)-3-hydroxytetrahydrofuran, and its (R)-enantiomer, from malic or tartaric acid, *J. Org. Chem.*, 1983, **48**, 2767–2769.
- 85 T. Iqbal, Q. Lu, C. Dong, M. Zhou, Z. Arain, Z. Ali, I. Khan, Z. Hussain and A. Abbas, in 2018 International Conference on Computing, Mathematics and Engineering Technologies (iCoMET), 2018, pp. 1–6.

- 86 A. Yu. Sidorenko, Yu. M. Kurban, A. Aho, Zh. V. Ihnatovich, T. F. Kuznetsova, I. Heinmaa, D. Yu. Murzin and V. E. Agabekov, Solvent-free synthesis of tetrahydropyran alcohols over acid-modified clays, *Mol. Catal.*, 2021, 499, 111306.
- 87 Z. J. Brentzel, K. J. Barnett, K. Huang, C. T. Maravelias, J. A. Dumesic and G. W. Huber, Chemicals from Biomass: Combining Ring-Opening Tautomerization and Hydrogenation Reactions to Produce 1,5-Pentanediol from Furfural, *Chemsuschem*, 2017, **10**, 1351–1355.
- 88 B. Lasne, P. Mäki-Arvela, A. Aho, Z. Vajglova, K. Eränen, N. Kumar, J. E. Sánchez-Velandia, M. Peurla, C. Mondelli, J. Pérez-Ramírez and D. Y. Murzin, Synthesis of Florol via Prins cyclization over heterogeneous catalysts, *J. Catal.*, 2022, **405**, 288–302.
- 89 M. Dahmen and W. Marquardt, Model-Based Design of Tailor-Made Biofuels, *Energy Fuels*, 2016, **30**, 1109–1134.
- 90 C. L. Yaws, Yaws' Handbook of Thermodynamic Properties for Hydrocarbons and Chemicals.
- 91 Burgess, Donald R., in *NIST Chemistry WebBook, NIST Standard Reference Database Number 69*, eds. P. J. Linstrom and W. G. Mallard, National Institute of Standards and Technology.
- 92 S. Brunauer, P. H. Emmett and E. Teller, Adsorption of Gases in Multimolecular Layers, *J. Am. Chem. Soc.*, 1938, **60**, 309–319.
- 93 X. Gao, A. Heyden, O. A. Abdelrahman and J. Q. Bond, Microkinetic analysis of acetone hydrogenation over Pt/SiO2, *J. Catal.*, 2019, **374**, 183–198.
- 94 R. A. D. Betta, Measurement of ruthenium metal surface area by chemisorption, *J. Catal.*, 1974, **34**, 57–60.
- 95 M. F. Brown and R. D. Gonzalez, An infrared study of the adsorption of carbon monoxide on the reduced and oxidized forms of silica supported ruthenium, *J. Phys. Chem.*, 1976, **80**, 1731–1735.
- 96 H. M. Miura, M. L. McLaughlin and R. D. Gonzalez, The coadsorption of CO and H2 on silica-supported Ru catalysts, *J. Catal.*, 1983, **79**, 227–232.
- 97 A. A. Davydov and A. T. Bell, An infrared study of NO and CO adsorption on a silica-supported Ru catalyst, *J. Catal.*, 1977, **49**, 332–344.
- 98 H. Miura and R. D. Gonzalez, Methanation studies over well-characterized silica-supported Pt-Ru bimetallic clusters, *J. Catal.*, 1982, **74**, 216–224.
- 99 R. Ahlrichs, M. Bär, M. Häser, H. Horn and C. Kölmel, Electronic structure calculations on workstation computers: The program system turbomole, *Chem. Phys. Lett.*, 1989, **162**, 165–169.
- 100 O. Treutler and R. Ahlrichs, Efficient molecular numerical integration schemes, *J. Chem. Phys.*, 1995, **102**, 346–354.
- 101 M. Von Arnim and R. Ahlrichs, Performance of parallel TURBOMOLE for density functional calculations, *J. Comput. Chem.*, 1998, **19**, 1746–1757.
- 102 J.-D. Chai and M. Head-Gordon, Long-range corrected hybrid density functionals with damped atom—atom dispersion corrections, *Phys. Chem. Chem. Phys.*, 2008, **10**, 6615.
- 103 F. Weigend, M. Häser, H. Patzelt and R. Ahlrichs, RI-MP2: optimized auxiliary basis sets and demonstration of efficiency, *Chem. Phys. Lett.*, 1998, **294**, 143–152.
- 104F. Weigend and R. Ahlrichs, Balanced basis sets of split valence, triple zeta valence and quadruple zeta valence quality for H to Rn: Design and assessment of accuracy, *Phys. Chem. Chem. Phys.*, 2005, **7**, 3297.

- 105 F. Weigend, Accurate Coulomb-fitting basis sets for H to Rn, *Phys. Chem. Chem. Phys.*, 2006, **8**, 1057.
- 106K. Eichkorn, O. Treutler, H. Öhm, M. Häser and R. Ahlrichs, Auxiliary basis sets to approximate Coulomb potentials, *Chem. Phys. Lett.*, 1995, **240**, 283–290.
- 107 K. Eichkorn, F. Weigend, O. Treutler and R. Ahlrichs, Auxiliary basis sets for main row atoms and transition metals and their use to approximate Coulomb potentials, *Theor. Chem. Acc. Theory Comput. Model. Theor. Chim. Acta*, 1997, **97**, 119–124.
- 108 P. Deglmann and F. Furche, Efficient characterization of stationary points on potential energy surfaces, *J. Chem. Phys.*, 2002, **117**, 9535–9538.
- 109 P. Deglmann, F. Furche and R. Ahlrichs, An efficient implementation of second analytical derivatives for density functional methods, *Chem. Phys. Lett.*, 2002, **362**, 511–518.
- 110G. Kresse and J. Hafner, *Ab initio* molecular dynamics for liquid metals, *Phys. Rev. B*, 1993, 47, 558–561.
- 111 G. Kresse and J. Hafner, *Ab initio* molecular-dynamics simulation of the liquid-metal–amorphous-semiconductor transition in germanium, *Phys. Rev. B*, 1994, **49**, 14251–14269.
- 112 P. E. Blöchl, Projector augmented-wave method, *Phys. Rev. B*, 1994, **50**, 17953–17979.
- 113 J. P. Perdew and W. Yue, Accurate and simple density functional for the electronic exchange energy: Generalized gradient approximation, *Phys. Rev. B*, 1986, **33**, 8800–8802.
- 114J. P. Perdew and Y. Wang, Accurate and simple analytic representation of the electron-gas correlation energy, *Phys. Rev. B*, 1992, **45**, 13244–13249.
- 115 S. Grimme, J. Antony, S. Ehrlich and H. Krieg, A consistent and accurate *ab initio* parametrization of density functional dispersion correction (DFT-D) for the 94 elements H-Pu, *J. Chem. Phys.*, 2010, **132**, 154104.
- 116J. Harris, Simplified method for calculating the energy of weakly interacting fragments, *Phys. Rev. B*, 1985, **31**, 1770–1779.
- 117 W. M. C. Foulkes and R. Haydock, Tight-binding models and density-functional theory, *Phys. Rev. B*, 1989, **39**, 12520–12536.
- 118G. Makov and M. C. Payne, Periodic boundary conditions in *ab initio* calculations, *Phys. Rev. B*, 1995, **51**, 4014–4022.
- 119 H. J. Monkhorst and J. D. Pack, Special points for Brillouin-zone integrations, *Phys. Rev. B*, 1976, **13**, 5188–5192.
- 120 M. Methfessel and A. T. Paxton, High-precision sampling for Brillouin-zone integration in metals, *Phys. Rev. B*, 1989, **40**, 3616–3621.
- 121 J. W. Arblaster, Crystallographic Properties of Ruthenium, *Platin. Met. Rev.*, 2013, **57**, 127–136.
- 122 G. Henkelman and H. Jónsson, Improved tangent estimate in the nudged elastic band method for finding minimum energy paths and saddle points, *J. Chem. Phys.*, 2000, **113**, 9978–9985.
- 123 G. Henkelman and H. Jónsson, A dimer method for finding saddle points on high dimensional potential surfaces using only first derivatives, *J. Chem. Phys.*, 1999, **111**, 7010–7022.
- 124G. Henkelman, B. P. Uberuaga and H. Jónsson, A climbing image nudged elastic band method for finding saddle points and minimum energy paths, *J. Chem. Phys.*, 2000, **113**, 9901–9904.
- 125 N. L. Haworth, Q. Wang and M. L. Coote, Modeling Flexible Molecules in Solution: A p *K* ^a Case Study, *J. Phys. Chem. A*, 2017, **121**, 5217–5225.

- 126J. A. Dumesic, Analyses of reaction schemes using De Donder relations, *J. Catal.*, 1999, **185**, 496–505.
- 127 T. J. Schwartz and J. Q. Bond, Leveraging De Donder relations for a thermodynamically rigorous analysis of reaction kinetics in liquid media, *J. Catal.*, 2021, **404**, 687–705.
- 128 L. Bui and A. Bhan, Mechanisms for CC bond cleavage and formation during acrolein production on a mixed metal oxide catalyst, *Appl. Catal. Gen.*, 2017, **546**, 87–95.
- 129 D. Ruiz, A. Aho, T. Saloranta, K. Eränen, J. Wärnå, R. Leino and D. Yu. Murzin, Direct amination of dodecanol with NH3 over heterogeneous catalysts. Catalyst screening and kinetic modelling, *Chem. Eng. J.*, 2017, **307**, 739–749.
- 130 J. Gopeesingh, R. Zhu, R. Schuarca, W. Yang, A. Heyden and J. Q. Bond, Kinetic and Mechanistic Analysis of the Hydrodeoxygenation of Propanoic Acid on Pt/SiO2, *Ind. Eng. Chem. Res.*, 2021, **60**, 16171–16187.
- 131 K. Shimizu, S. Kanno, K. Kon, S. M. A. Hakim Siddiki, H. Tanaka and Y. Sakata, Nalkylation of ammonia and amines with alcohols catalyzed by Ni-loaded CaSiO3, *Catal. Today*, 2014, **232**, 134–138.
- 132 K. Shimizu, K. Kon, W. Onodera, H. Yamazaki and J. N. Kondo, Heterogeneous Ni Catalyst for Direct Synthesis of Primary Amines from Alcohols and Ammonia, *ACS Catal.*, 2013, **3**, 112–117.